Application of Rayleigh-Ritz formulation to thermomechanical buckling of variable angle tow composite plates with general in-plane boundary constraint

Xiaodong Chen[1,*] Guojun Nie[2,†] Zhangming Wu[3,4,‡]

[1] School of Civil and Transportation Engineering, Henan University of Urban Construction, Pingdingshan 467000, China
[2] School of Aerospace Engineering and Applied Mechanics, Tongji University, Shanghai 200092, China
[3] School of Mechanical Engineering and Mechanics, Ningbo University, Ningbo 315211, China
[4] Cardifff School of Engineering, Cardiff University, Cardiff CF24 3AA, UK

Abstract

Variable Angle Tow (VAT) composites always exhibit in-plane variable stiffness property, which provides the designer with an extended freedom in stiffness tailoring to achieve higher structural performance for lightweight composite structures. In this paper, a methodology based on a generalised Rayleigh-Ritz formulation is developed to study the thermomechanical buckling response of symmetrical VAT composite plates with general in-plane boundary constraint. It is assumed that the material is of temperature-independent and the panel is exposed to an arbitrary in-plane temperature change. In the framework of thermoelastic theory, the principle of thermoelastic complementary energy in conjunction with Airy's stress function formulation, for the first time, is applied to solve the in-plane thermoelastic problem of the tow-steered plate. The non-uniform distribution of in-plane force resultant over the entire plane is determined by utilizing the Rayleigh-Ritz formulation enhanced by Lagrangian multiplier method. The merit of the proposed modelling strategy lies in that the application of Lagrangian multiplier method removes the restrictions inherent in conventional Rayleigh-Ritz formulation and thus provides generality to model general in-plane boundary constraint against thermal expansion or contraction. During the buckling analysis, the governing equation of thermomechanical buckling problem of the tow-steered plate under a combination of both

*E-mail address: 1263895177@qq.com (Xiaodong Chen, Corresponding author)
†E-mail address: ngj@tongji.edu.cn (Guojun Nie)
‡E-mail address: zhangming.wu@nbu.edu.cn; wuz12@cardiff.ac.uk(Zhangming Wu)

temperature change and general in-plane boundary constraint is derived based on the third-order shear deformation theory of Reddy's type. The accuracy and robustness of the proposed Rayleigh-Ritz model is validated against finite element solutions and previously published results. Effects of boundary condition, fibre orientation angle and temperature change on the in-plane thermoelastic and thermomechanical buckling behaviours of VAT composite plates are studied by numerical examples. Finally, the mechanism of applying tow-steered technology to improve the thermomechanical buckling resistance of composite plates is explored.
Keywords: Variable angle tow, Thermomechanical buckling, Rayleigh-Ritz method, Airy's stress function, The principle of thermoelastic complementary energy, Third-order shear deformation theory

---

1. Introduction

Variable angle tow placement technology allows fibre orientations to continuously vary with position over the entire plane of each ply, which provides the designer of aircrafts with a considerable opportunities in stiffness tailoring to design lightweight composite structures with enhanced performance. Previous studies [1, 2, 3, 4, 5, 6, 7, 8, 9] reveal that substantial improvement in buckling performance can be obtained by appropriately steering fibre path over each ply of the panel and the reason for this enhanced performance is mainly attributed to benign load redistribution offered by the VAT layup configuration. However, an experimental investigation conducted by Wu et al. [10] has shown that residual thermal stresses induced by cooling the panel from high curing temperature to room temperature play a key role in the accurate evaluation of buckling response of variable stiffness composite panels. On the other hand, it had been well established that the wings of aircrafts when flying at supersonic speeds are prone to be aerodynamically heated from room temperature to high working temperature, which may lead to premature buckling of the skin [11]. In view of this, composite plates should be designed to operate in a certain range of temperature so as to increase structural efficiency. Therefore, there remains a strong demand for having an insight into the thermoelastic buckling behaviour of VAT composite plates exposed to temperature change.

A considerable amount of research effort has been devoted to the study of thermoelastic buckling problem of isotropic or straight-fibre composite plates undergoing uniform or nonuniform temperature change. In earlier stage, research works of thermal buckling problem mainly focused on isotropic plates [12, 13, 14, 15, 16, 11]. For instance, Gossard, Seide and Roberts [12] initially conducted a theoretical and experimental investigation on thermal buckling of isotropic plates subjected to a tent-like temperature distribution. In their work, the Rayleigh-Ritz energy method was applied to determine the critical buckling temperature of isotropic plates with all edges restrained against normal expansion, while the Galerkin method was applied to solve the strong-form partial differential equation derived from the von Kármán large-deflection theory during the postbuckling stage. Later, Hoff [13, 14] studied the thermal buckling behaviour of the cover plate bounded by two shear webs in supersonic wing structure. Prabhu and Durvasula [15] applied the Galerkin method to perform the thermal buckling analysis of skew plates with all edges restrained against expansion. The Galerkin method was also used in the work of Chen et al. [16], in which the thermal stability problem of a transversely isotropic thick plate with thermal effects in a general state of nonuniform initial stress was solved. Bargmann [11] adopted Airy's stress function expressed by infinite harmonic series to derive the expression of thermal stress distribution acting on an isotropic plate and discussed the thermal buckling response of initially stress-free, elastic plates under nonuniform temperature field. On the other hand, the study on thermal buckling problem has also been extended to straight-fibre composite plates by several researchers. Whitney and Ashton [17] applied the generalized Duhamel-Neumann form of Hooke's law to derive displacement-based governing equations including the effect of expansional strains induced by temperature and humidity and investigated the thermal buckling response of layered composite plates with all edges restrained against normal expansions. Tauchert and Huang [18] applied the Rayleigh-Ritz energy method to solve the thermal buckling problem of symmetric angle-ply laminated plates subjected to a uniform temperature change. Meryers and Hyer [19] extended the work of Tauchert and Huang [18] to study the thermal buckling and postbuckling response of symmetrically laminated composite plates. Sun and Hsu [20] presented a Navier solution of critical buckling temperature for simply supported, symmetric cross-ply laminates including the effect of transverse shear under uniform temperature distribution. Librescu et al. [21] investigated the static postbuckling of simply-supported flat panels exposed to a stationary nonuniform temperature field and subjected 'to a system of subcritical in-plane compressive edge loads. Dona and

Hyer [22] developed a theoretical model based on a Rayleigh-Ritz minimization of the total potential energy to predict thermally induced deformation behavior of general unsymmetric laminates. Shen [23] studied the thermomechanical postbuckling response of imperfect laminated plates using a higher-order shear deformation theory. Jones [24] employed the equivalent mechanical loading concept to derive simple solutions to the most fundamental thermal buckling problems for uniformly heated unidirectional and symmetric cross-ply laminated fibre-reinforced composite rectangular plates. Shariyat [25] investigated the thermal buckling analysis of rectangular composite multilayered plates with temperature-dependent properties under uniform temperature rise using the layerwise plate theory. Recently, Li [26] derived an analytical solution of thermal buckling response of the composite laminated plate under fully clamped boundary condition. Cetkovic [27] applied layerwise displacement model to derive both finite element and closed-form solution for the thermal buckling analysis of laminated composite plates. Tran et al. [28] employed isogeometric approach to study the thermal bending and buckling analyses of laminated composite plates. Gutiérrez Álvarez and Bisagni [29] derived a closed-form solution for thermomechanical buckling of orthotropic composite plates under the effect of thermal and mechanical loads. In addition, the thermoelastic buckling response of the straight-fibre plate was also widely investigated by using finite element approach [30, 31, 32, 33]. Based on the previous literature survey, it appears that for isotropic or straight-fibre plates with symmetric layups, the prebuckling analysis is required to determine the distribution of in-plane stress resultant before the thermoelastic buckling analysis, especially for the plates undergoing nonuniform temperature change. Closed-form solutions of prebuckling resultants for some specific cases can be found in the woks of Sun and Hsu [20], Tauchert and Huang [18], Meryers and Hyer [19], Li et al. [26] and Gutiérrez Álvarez and Bisagni [29]. For more general cases, however, the analytical methods based on a variational principle such as Rayleigh-Ritz energy method may offer an efficient means to analyse in-plane thermoelastic behaviour of isotropic or composite plates. In previous works [18, 19], the prebuckling problem was solved by minimising the potential energy expressed in terms of two unknown displacement variables. However, the resulting weak-form solution fails to satisfy the natural (or force) boundary conditions along four edges of the plate [18]. Airy's stress function formulation, in the framework of thermoelastic theory, is much more convenient for dealing with various in-plane boundary conditions than using the displacement function formulation, especially for pure stress or mixed (stress and displacement) boundary constraints [34, 35, 11]. Therefore, in the present work, Airy's stress function formulation is employed to represent the in-plane force resultant component. Furthermore, the first variation of the thermoelastic complementary energy expressed in terms of Airy's stress function formulation, for the first time, is applied to solve the prebuckling problem of symmetric composite plates exposed to temperature change.

On the other hand, a considerable research works have been done on buckling of variable stiffness composite plates induced by mechanical loadings. Hyer et al. [36, 37] initially used curvilinear fibre paths aligned along the principal directions of the stress fields to improve the buckling resistance of composite panel with a central hole. Later, Gürdal and his coworkers [38, 39] conducted a theoretical investigation on the in-plane stress and buckling behaviours of variable stiffness laminates. They employed a numerical tool (ELLPACK) to directly solve a set of coupled elliptic partial differential equations for the in-plane stress problem and applied the Rayleigh–Ritz method to deal with the eigenvalue equations for the buckling problem. Following the pioneering works of Gürdal et al [38, 39], several semi-analytical and reduced order models were developed to study enhanced buckling behaviors of VAT composite plates. Wu et al. [3, 40, 41] applied the Rayleigh-Ritz method to determine the buckling behaviour of VAT composite plates subjected to compression loadings. Raju et al. [4, 42] developed a numerical methodology based on the Differential Quadrature Method (DQM) for the prebuckling, buckling and postbuckling analysis of VAT composite panels. Zucco et al. [43] developed a mixed quadrilateral 3D finite element based on the Hellinger–Reissner variational principle for linear static and buckling analyses of VAT composite plates under constant shear loading or compression loading. In addition, Coburn et al. [44] and Oliveri and Milazzo [45] studied the buckling response of stiffened VAT panels. Chen et al. [7] investigated the buckling behaviour of VAT composite plates with delamination. Vescovini et al. [46] developed a semi-analytical method for the analysis of composite stiffened panels where stiffness variability is achieved through a combination of fiber steering and curvilinear stringers. Although buckling of VAT composite plates or structures under mechanical loadings has been extensively studied, the thermoelastic buckling of VAT composite plates or structures has received little attention. Recently, Haldar et al. [47] extended the Rayleigh-Ritz minimization technique proposed by Dano and Hyer [22] to study thermally induced multistable behavior of unsymmetric laminates with curvilinear fibre paths. Vescovini and Dozio [48] studied the thermal buckling of VAT composite plates in the framework of a variable-kinematics approach based on Carrera's Unified Formulation (CUF). In their work, closed-form solutions of prebuckling results are presented four different sets of in-plane boundary constraints. Other works [49, 50, 51, 52, 53, 54, 55, 56] on thermal buckling analysis of VAT composite plates or structures mainly relied on the finite element approach, in which a significant computational effort was required to solve the thermal buckling problem, especially coupled with optimisation algorithms. To the best of the authors' knowledge, no research has been published in which an attempt has been made to study the thermomechanical buckling behaviour of VAT plates with general in-plane boundary constraint. Actually, the plate edges may be partially or completely restrained against thermal expansion or contraction, and in particular scenarios, may be even free of external forces. Therefore, to explore an effective modeling strategy for dealing with general in-plane boundary constraint is of crucial importance to fully understand the thermoelastic behavior of composite plates, especially enhanced with curvilinear fibre path. In the present work, an efficient model based on a generalised Rayleigh-Ritz energy method is developed to study the thermomechanical buckling behaviour of VAT composite panels with general boundary constraint. The merit of the proposed modelling strategy lies in that the Lagrangian multiplier method is applied to remove the restrictions on admissibility requirement inherent in conventional Rayleigh-Ritz formulation, which provides generality to model general in-plane boundary constraint against thermal expansion or contraction.

The content of this paper is arranged as follows. In the next section, the concept of VAT laminates is introduced. Section 3 presents the theoretical formulation for both prebuckling and thermomechanical buckling problems of VAT composite plates under a combination of temperature change and general boundary constraint. In Section 4, the accuracy and reliability of the proposed Rayleigh-Ritz energy model are validated by finite element analysis and with prior results. Effects of boundary condition, fibre orientation angle and temperature change on the in-plane thermoelastic and thermomechanical buckling behaviours of VAT composite plates are studied by numerical examples. The mechanism of exploiting variable stiffness properties to improve the thermomechanical buckling resistance of composite plates is also explored. Finally, some conclusions are drawn in Section 5.

2. VAT laminates

The orientation of fibre angles of each ply of the VAT composite plate are continuously varied with respect to the coordinates x and y, which has the dual purpose of representing variable stiffness properties. As such, VAT composite plates provide extended design flexibility to potentially enhance structural performance. Generally, the fibre angle variation of a VAT plate is represented in a mathematical form using a small number of fibre angle parameters [3]. In this work, for simplicity, the VAT plate with a linear fibre angle variation is considered, as shown in Fig. 1, and the angle variation along the x' direction is [1]

$$\theta(x') = \phi + \frac{(T_1 - T_0)}{d} \mid x' \mid + T_0 \quad \text{with} \quad x' = x\cos\phi + y\sin\phi \tag{1}$$

where T_0 and T_1 are fibre orientation angles at two prescribed reference points. d is the distance between the starting and ending points; ϕ is the angle of rotation of the fibre path. In the present work, two types of laminates are considered, that is, $\phi = 0°$ and $\phi = 90°$. The layup configuration for the VAT laminates can be characterised by $[\phi\langle T_0|T_1\rangle]$.

3. Theoretical formulation

3.1. Legendre polynominals

Compared to other orthogonal and complete series such as trigonometric Fourier series and beam functions, the Legendre polynomials always exhibit better convergence and stability in capturing local response of composite structures [3, 7, 9]. In the present work, the Legendre polynomials are therefore adopted to characterize the admissible functions implemented in the Rayleigh-Ritz formulation and defined as:

$$\begin{aligned} L_0(x) &= 1 \\ L_1(x) &= x \\ L_p(x) &= \frac{2p-1}{p} x L_{p-1}(x) - \frac{p-1}{p} L_{p-2}(x), \quad p = 2, 3, ... \end{aligned} \tag{2}$$

where p is the polynomial degree. This set of polynomials represents an orthonormal basis, and their roots are identical with integration points of Gauss quadrature rules. They also satisfy the Legendre differential equation.

3.2. Prebuckling analysis

In the present work, the material properties of the plate are assumed to do not vary with temperature, that is, the material is of temperature-independent. On the other hand, it is assumed that there exists no variation in temperature through the thickness of the plate, that is, the temperature is independent of the thickness direction, which is reasonable when the speed of flight does not exceed Mach Numbers of 3 or 4 [13]. Note that, if this is not the case, the panel will, in general, not remain plane and thus lead to the occurrence of bending and/or twisting moments within the panel [35, 57], which is beyond the scope of this paper. However, the panel considered is exposed to an arbitrary in-plane temperature distribution $\Delta T(x, y)$. The problem is thus one of generalised plane stress. For symmetric VAT composite plates, the relationship between in-plane and out-of-plane behaviours within the plate is uncoupled. Therefore, the plane-stress stress-strain relations with free thermal strain effects included can be expressed using

$$\begin{Bmatrix} \varepsilon_x^0 \\ \varepsilon_y^0 \\ \gamma_{xy}^0 \end{Bmatrix} = \begin{bmatrix} a_{11}(x,y) & a_{12}(x,y) & a_{16}(x,y) \\ a_{12}(x,y) & a_{22}(x,y) & a_{26}(x,y) \\ a_{16}(x,y) & a_{26}(x,y) & a_{66}(x,y) \end{bmatrix} \begin{Bmatrix} N_x^0 \\ N_y^0 \\ N_{xy}^0 \end{Bmatrix} + \begin{Bmatrix} \varepsilon_x^{th} \\ \varepsilon_y^{th} \\ \gamma_{xy}^{th} \end{Bmatrix} \tag{3}$$

where $a_{ij}(i, j = 1, 2, 6)$ are the in-plane compliance coefficients [58]; N_x^0, N_y^0 and N_{xy}^0 are the in-plane force resultants; ε_x^0, ε_y^0 and γ_{xy}^0 are the in-plane total strains, while ε_x^{th}, ε_y^{th} and γ_{xy}^{th} are the in-plane thermal strains. The in-plane mechanical strains ε_x^{me}, ε_y^{me} and γ_{xy}^{me} are then represented as $\varepsilon_x^0 - \varepsilon_x^{me}$, $\varepsilon_y^0 - \varepsilon_y^{me}$ and $\gamma_{xy}^0 - \gamma_{xy}^{me}$, respectively.

The in-plane thermal strains (ε_x^{th}, ε_y^{th} and γ_{xy}^{th}) within the plate are expressed as

$$\begin{Bmatrix} \varepsilon_x^{th} \\ \varepsilon_y^{th} \\ \gamma_{xy}^{th} \end{Bmatrix} = \begin{bmatrix} a_{11}(x,y) & a_{12}(x,y) & a_{16}(x,y) \\ a_{12}(x,y) & a_{22}(x,y) & a_{26}(x,y) \\ a_{16}(x,y) & a_{26}(x,y) & a_{66}(x,y) \end{bmatrix} \begin{Bmatrix} N_x^{th} \\ N_y^{th} \\ N_{xy}^{th} \end{Bmatrix} \tag{4}$$

with

$$\begin{Bmatrix} N_x^{th} \\ N_y^{th} \\ N_{xy}^{th} \end{Bmatrix} = \sum_{k=0}^{K} \int_{z_{k-1}}^{z_k} \begin{bmatrix} Q_{11}^k(x,y) & Q_{12}^k(x,y) & Q_{16}^k(x,y) \\ Q_{12}^k(x,y) & Q_{22}^k(x,y) & Q_{26}^k(x,y) \\ Q_{16}^k(x,y) & Q_{26}^k(x,y) & Q_{66}^k(x,y) \end{bmatrix} \begin{Bmatrix} \alpha_x^k(x,y)\Delta T \\ \alpha_y^k(x,y)\Delta T \\ \alpha_{xy}^k(x,y)\Delta T \end{Bmatrix} \mathrm{d}z \tag{5}$$

where N_x^{th}, N_y^{th} and N_{xy}^{th} are the in-plane thermal force resultants; α_x^k, α_y^k and α_{xy}^k are the thermal expansion coefficients of the k^{th} layer of the plate, which can be expressed as

$$\begin{aligned} \alpha_x^k(x,y) &= \alpha_1 \cos^2\theta^k(x,y) + \alpha_2 \sin^2\theta^k(x,y) \\ \alpha_y^k(x,y) &= \alpha_1 \sin^2\theta^k(x,y) + \alpha_2 \cos^2\theta^k(x,y) \\ \alpha_{xy}^k(x,y) &= 2(\alpha_1 - \alpha_2)\sin\theta^k(x,y)\cos\theta^k(x,y) \end{aligned} \tag{6}$$

where α_1 and α_2 are the thermal expansion coefficients along the principal directions of the material [58].

In the framework of thermoelastic theory, both the in-plane equilibrium equation and compatibility condition require to be simultaneously satisfied in the derivation of the governing equation [35]. The Airy's stress function Φ, which automatically satisfies the in-plane equilibrium equations [34, 35, 59, 11], is thus introduced to represent the in-plane force resultants (N_x^0, N_y^0 and N_{xy}^0), that is,

$$N_x^0 = \frac{\partial^2\Phi}{\partial y^2}, \quad N_y^0 = \frac{\partial^2\Phi}{\partial x^2}, \quad N_{xy}^0 = -\frac{\partial^2\Phi}{\partial x\partial y} \tag{7}$$

Additionally, in the framework of thermoelastic theory [35], the compatibility condition of the plate is described in terms of the in-plane total strains (ε_x^0, ε_y^0 and γ_{xy}^0) instead of the in-plane thermal strains (ε_x^{th}, ε_y^{th} and γ_{xy}^{th}) or mechanical strains (ε_x^{me}, ε_y^{me} and γ_{xy}^{me}) . In view of the plane-stress state, the compatibility condition of the plate can be expressed using

$$\frac{\partial^2\varepsilon_x^0}{\partial y^2} + \frac{\partial^2\varepsilon_y^0}{\partial y^2} - \frac{\partial^2\gamma_{xy}^0}{\partial x\partial y} = 0 \tag{8}$$

Substituting Eqs. 3, 4 and 7 into Eq. 8, the compatibility equation expressed in terms of

Airy's stress function for the tow-steered plate is obtained as follows,

$$
\begin{aligned}
&\frac{\partial^2}{\partial y^2}[a_{11}(x,y)\Phi_{,yy} + a_{12}(x,y)\Phi_{,xx} - a_{16}(x,y)\Phi_{,xy}] + \\
&\frac{\partial^2}{\partial x^2}[a_{12}(x,y)\Phi_{,yy} + a_{22}(x,y)\Phi_{,xx} - a_{26}(x,y)\Phi_{,xy}] - \\
&\frac{\partial^2}{\partial x \partial y}[a_{16}(x,y)\Phi_{,yy} + a_{26}(x,y)\Phi_{,xx} - a_{66}(x,y)\Phi_{,xy}] = -\Omega^*(x,y)
\end{aligned}
\tag{9}
$$

with

$$
\begin{aligned}
\Omega^*(x,y) = &\frac{\partial^2}{\partial y^2}[a_{11}(x,y)N_x^{th} + a_{12}(x,y)N_y^{th} + a_{16}(x,y)N_{xy}^{th}] \\
&+ \frac{\partial^2}{\partial x^2}[a_{12}(x,y)N_x^{th} + a_{22}(x,y)N_y^{th} + a_{26}(x,y)N_{xy}^{th}] \\
&- \frac{\partial^2}{\partial x \partial y}[a_{16}(x,y)N_x^{th} + a_{26}(x,y)N_y^{th} + a_{66}(x,y)N_{xy}^{th}]
\end{aligned}
\tag{10}
$$

where a comma denotes differentiation of the Airy's stress function with respect to the subscript. In particular, for the case of no external forces on four edges, the in-plane stress boundary conditions of the plate can be directly expressed in terms of the Airy's stress function Φ, as shown in Eq. 11, which are found to be of homogeneous type.

$$
\begin{aligned}
x = \pm a/2: &\quad \Phi_{,yy}(\pm a/2, y) = 0 \quad \Phi_{,xy}(\pm a/2, y) = 0 \\
y = \pm b/2: &\quad \Phi_{,xx}(x, \pm b/2) = 0 \quad \Phi_{,xy}(x, \pm b/2) = 0
\end{aligned}
\tag{11}
$$

The above compatibility equation and its corresponding stress boundary condition, which govern the in-plane thermoelastic problem of the tow-steered plate undergoing an arbitrary temperature change $\Delta T(x,y)$, constitute a typical boundary value problem of Partial Differential Equation (PDE). Expanding the derivatives in Eq. 9, it was found that the compatibility equation involves additional higher order derivative terms with respect to the in-plane flexibility $a_{ij}(i,j=1,2,6)$. For straight-fibre plates under uniform temperature rise or drop ($\Delta T(x,y) \equiv \Delta\overline{T}$), both the in-plane thermal force resultants (N_x^{th}, N_y^{th} and N_{xy}^{th}) and compliance coefficients $a_{ij}(i,j=1,2,6)$ remain constant over the entire panel. As such, the compatibility equation in Eq. 9 tends to be homogeneous ($\Omega^*(x,y) \equiv 0$), which means that there exists no in-plane force resultants (N_x^0, N_y^0 and N_{xy}^0) over the entire plane of the plate. Under such circumstance, the plate uniformly expand or contract due to the temperature rise or drop. However, for VAT plates under uniform temperature change or straight-fibre plates under nonuniform temperature change, the function $\Omega^*(x, y)$ on the right-hand side of Eq. 9 varies with respect to the coordinates x and y, and thus the compatibility equation in Eq. 9 becomes inhomogeneous, which will inevitably lead to the occurence of in-plane force resultants (N_x^0, N_y^0 and N_{xy}^0) within the plate domain. In these cases, one may directly solve the governing equation by applying several powerful mathematical methods such as Galerkin method [15], Differential Quadrature Method (DQM) [4, 60, 61], Complex Function Method (CFM) [62] and Fourier Series Method (FSM) [34, 35, 59]. In the present work, however, the Rayleigh-Ritz formulation based on the weak-form variational principle is adopted to deal with the in-plane thermoelastic problem of the VAT plate under an arbitrary temperature change $\Delta T(x, y)$. The obvious advantages of this approach lie in that the derivative terms of stiffness coefficients are avoided, and this leads to the analysis procedure for a VAT laminate analogous to a constant stiffness laminate [41]. Huang and Tauchert [18] and Meyers and Hyer [19] solved the in-plane thermoelastic problem of straight-fibre plates under temperature change through the first variation of the total thermoelastic strain energy or potential energy, which are expressed in terms of two unknown displacement fields (u^0 and v^0),

$$\delta\Pi_P(u^0, v^0) = \iint\limits_{\Omega} \left[(N_x^{tot} - N_x^{th})\delta\varepsilon_x^0 + (N_y^{tot} - N_y^{th})\delta\varepsilon_y^0 + (N_{xy}^{tot} - N_{xy}^{th})\delta\gamma_{xy}^0\right]\mathrm{d}x\mathrm{d}y \tag{12}$$

A more detailed description of the expanded form in Eq. 12 can be found in Refs. [18] and [19]. However, the resulting weak-form solution fails to satisfy the natural (or force) boundary conditions along four edges of the plate [18]. To this aim, the first variation of the thermoelastic complementary energy of the plate is thus adopted in the present work and written as follows [63]:

$$\delta\Pi_C(\Phi) = \iint\limits_{\Omega} \left[(\varepsilon_x^{me} + \varepsilon_x^{th})\delta N_x^0 + (\varepsilon_y^{me} + \varepsilon_y^{th})\delta N_y^0 + (\gamma_{xy}^{me} + \gamma_{xy}^{th})\delta N_{xy}^0\right]\mathrm{d}x\mathrm{d}y \tag{13}$$

which can be expanded as,

$$\begin{aligned}\delta\Pi_C(\Phi) = \iint\limits_{\Omega} \Big[&\big(a_{11}(x,y)\frac{\partial^2\Phi}{\partial y^2} + a_{12}(x,y)\frac{\partial^2\Phi}{\partial x^2} - a_{16}(x,y)\frac{\partial^2\Phi}{\partial x\partial y}\big)\delta\frac{\partial^2\Phi}{\partial y^2} \\ &+ \big(a_{12}(x,y)\frac{\partial^2\Phi}{\partial y^2} + a_{22}(x,y)\frac{\partial^2\Phi}{\partial x^2} - a_{26}(x,y)\frac{\partial^2\Phi}{\partial x\partial y}\big)\delta\frac{\partial^2\Phi}{\partial x^2} \\ &- \big(a_{16}(x,y)\frac{\partial^2\Phi}{\partial y^2} + a_{26}(x,y)\frac{\partial^2\Phi}{\partial x^2} - a_{66}(x,y)\frac{\partial^2\Phi}{\partial x\partial y}\big)\delta\frac{\partial^2\Phi}{\partial x\partial y} \\ &+ \big(\varepsilon_x^{th}(x,y)\delta\frac{\partial^2\Phi}{\partial y^2} + \varepsilon_y^{th}(x,y)\delta\frac{\partial^2\Phi}{\partial x^2} - \gamma_{xy}^{th}(x,y)\delta\frac{\partial^2\Phi}{\partial x\partial y}\big)\Big]\mathrm{d}x\mathrm{d}y\end{aligned} \tag{14}$$

In the Rayleigh-Ritz formulation, the Airy's stress function Φ can be constructed by employing admissible functions that fully satisfy the stress-free boundary conditions along four edges of the panel (see Eq. 11) and is thus expressed as [3, 64, 9]

$$\Phi(\xi,\eta) = (1-\xi^2)^2(1-\eta^2)^2 \sum_{p=0}^{P}\sum_{q=0}^{Q}\phi_{pq}L_p(\xi)L_q(\eta) \tag{15}$$

where $\xi = 2x/a$ and $\eta = 2y/b$; $L_p(\xi)$ and $L_q(\eta)$ are the p^{th} and q^{th} Legendre polynomials with respect to ξ and η, respectively. By substituting Eqs. 7 and 15 into Eq. 14 and setting the first variation of the thermoelastic complementary energy $\delta\Pi_C(\phi_{pq})$ $(p = 0, 1, \cdots, P;\ q = 0, 1, \cdots, Q)$ to zero, that is,

$$\delta\Pi_C(\phi_{00}, \phi_{01}, \cdots, \phi_{PQ}) = 0 \tag{16}$$

a set of linear algebraic equations is then generated and expressed in the following matrix form:

$$\mathbf{K}\boldsymbol{\phi} = \boldsymbol{\Psi}^{th} \tag{17}$$

where $\mathbf{K}$ is the membrane stiffness matrix of the plate; $\boldsymbol{\Psi}^{th}$ is the thermally induced load vector. With the solution of Airy's stress function given by Eq. 15, the non-uniform in-plane force resultants (N_x^0, N_y^0 and N_{xy}^0) of the VAT plate under an arbitrary temperature change $\Delta T(x,y)$ can be determined from Eq. 7. It is noted that the weak-form equation (Eq. 17) based on the thermoelastic complementary energy principle is equivalent to the strong-form compatibility equation (Eq. 9). However, the linear governing equation given by Eq. 17 is only applicable to predict the in-plane thermoelastic response of the plate that is free of external forces on the edges. If the plate is further subjected to in-plane boundary constraints such as non-uniform shear loadings, combined normal and shear loadings or mixed stress and displacement loadings, an additional in-plane boundary condition requires to be considered in the Rayleigh-Ritz formulation. To this aim, the appropriate admissible functions need to be chosen in constructing the Airy's stress function Φ. Unfortunately, a challenging issue in the conventional Rayleigh-Ritz formulation lies in the implementation of complex in-plane boundary constraints. Recently, Chen and Nie [9] proposed an generalised Rayleigh-Ritz formulation enhanced by the Lagrangian multiplier method to successfully predict the in-plane response of VAT composite plates with general boundary constraints. With the aid of the Lagrangian multiplier method, the individual admissible functions need not satisfy the natural (or force) boundary conditions but the series as a whole is forced to satisfy these by introducing additional constraint equations, which greatly relaxes the admissibility requirement in the Rayleigh-Ritz formulation and is thus suitable to a more general in-plane boundary constraint. In the present work, the generalised Rayleigh-Ritz formulation proposed by Chen and Nie [9] is therefore extended to deal with the thermomechanical coupling problem of VAT composite plates with general in-plane boundary constraints. In the following, three kinds of in-plane boundary constraints are included, that is, pure stress boundary constraint (Case A), pure displacement boundary constraint (Case B) and mixed stress and displacement boundary constraint (Case C). Note, for each case, the panel is also exposed to an arbitrary temperature change $\Delta T(x, y)$.

Case A

In this subsection, the Rayleigh-Ritz formulation enhanced by the Lagrangian multiplier method is applied to solve the in-plane thermoelastic problem of VAT composite plates subjected to a combination of both temperature change and pure stress boundary constraints. The Airy's stress function Φ in the generalised Rayleigh-Ritz formulation is now redefined as:

$$\Phi(\xi, \eta) = \sum_{p=0}^{P} \sum_{q=0}^{Q} \phi_{pq} L_p(\xi) L_q(\eta) \tag{18}$$

Substituting Eq. 18 into Eq. 7, the in-plane force resultants N_x^0, N_y^0 and N_{xy}^0 in the framework of thermoelastic theory can then be expanded as:

$$\begin{aligned}
N_x^0 &= \frac{4}{b^2}\sum_{p=0}^{P}\sum_{q=2}^{Q}\phi_{pq}L_p(\xi)\frac{\partial^2 L_q(\eta)}{\partial\eta^2} \\
N_y^0 &= \frac{4}{a^2}\sum_{p=2}^{P}\sum_{q=0}^{Q}\phi_{pq}\frac{\partial^2 L_p(\xi)}{\partial\xi^2}L_q(\eta) \\
N_{xy}^0 &= -\frac{4}{ab}\sum_{p=1}^{P}\sum_{q=1}^{Q}\phi_{pq}\frac{\partial L_p(\xi)}{\partial\xi}\frac{\partial L_q(\eta)}{\partial\eta}
\end{aligned} \tag{19}$$

It is assumed that the prescribed boundary stress components ($\widetilde{N}_x^0$, $\widetilde{N}_y^0$ and $\widetilde{N}_{xy}^0$) along the edges ($\xi = \pm 1$, $\eta = \pm 1$) of the plate are known in advance. Then, we can easily obtain the following in-plane stress boundary conditions:

$$\begin{aligned}
\widetilde{N}_x^0(\eta)\Big|_{\xi=-1} &= \frac{4}{b^2}\sum_{q=2}^{Q}\Lambda_q^1\frac{\partial^2 L_q(\eta)}{\partial\eta^2}, \quad \widetilde{N}_x^0(\eta)\Big|_{\xi=1} = \frac{4}{b^2}\sum_{q=2}^{Q}\Lambda_q^2\frac{\partial^2 L_q(\eta)}{\partial\eta^2} \\
\widetilde{N}_y^0(\xi)\Big|_{\eta=-1} &= \frac{4}{a^2}\sum_{p=2}^{P}\Lambda_p^3\frac{\partial^2 L_p(\xi)}{\partial\xi^2}, \quad \widetilde{N}_y^0(\xi)\Big|_{\eta=1} = \frac{4}{a^2}\sum_{p=2}^{P}\Lambda_p^4\frac{\partial^2 L_p(\xi)}{\partial\xi^2} \\
\widetilde{N}_{xy}^0(\eta)\Big|_{\xi=-1} &= -\frac{4}{ab}\sum_{q=1}^{Q}\Lambda_q^5\frac{\partial L_q(\eta)}{\partial\eta}, \quad \widetilde{N}_{xy}^0(\eta)\Big|_{\xi=1} = -\frac{4}{ab}\sum_{q=1}^{Q}\Lambda_q^6\frac{\partial L_q(\eta)}{\partial\eta} \\
\widetilde{N}_{xy}^0(\xi)\Big|_{\eta=-1} &= -\frac{4}{ab}\sum_{p=1}^{P}\Lambda_p^7\frac{\partial L_p(\xi)}{\partial\xi}, \quad \widetilde{N}_{xy}^0(\xi)\Big|_{\eta=1} = -\frac{4}{ab}\sum_{p=1}^{P}\Lambda_p^8\frac{\partial L_p(\xi)}{\partial\xi}
\end{aligned} \tag{20}$$

with

$$\begin{aligned}
\Lambda_q^1 &= \sum_{p=0}^{P}\phi_{pq}L_p(-1), \quad \Lambda_q^2 = \sum_{p=0}^{P}\phi_{pq}L_p(1) \\
\Lambda_p^3 &= \sum_{q=0}^{Q}\phi_{pq}L_q(-1), \quad \Lambda_p^4 = \sum_{q=0}^{Q}\phi_{pq}L_q(1) \\
\Lambda_q^5 &= \sum_{p=1}^{P}\phi_{pq}\frac{\partial L_p(\xi)}{\partial\xi}\Big|_{\xi=-1}, \quad \Lambda_q^6 = \sum_{p=1}^{P}\phi_{pq}\frac{\partial L_p(\xi)}{\partial\xi}\Big|_{\xi=1} \\
\Lambda_p^7 &= \sum_{q=1}^{Q}\phi_{pq}\frac{\partial L_q(\eta)}{\partial\eta}\Big|_{\eta=-1}, \quad \Lambda_p^8 = \sum_{q=1}^{Q}\phi_{pq}\frac{\partial L_q(\eta)}{\partial\eta}\Big|_{\eta=1}
\end{aligned} \tag{21}$$

where Λ_j^i $(i = 1, 2, \cdots, 8;\ j = p, q)$ is defined as the *boundary stress coefficient*, which is related to the prescribed stress distribution on the i^{th} stress boundary condition. From Eq. 20, it is found that for each stress boundary condition, the corresponding boundary stress coefficient Λ_j^i $(i = 1, 2, \cdots, 8;\ j = p, q)$ can be determined by applying the appropriate mathematical fitting method and thus can be known in advance. From this point of view, Eq. 21 can be regarded as another form of the stress boundary constraint along the edges of the plate. In view of this, efforts must be concentrated on determining the boundary stress coefficient Λ_j^i $(i = 1, 2, \cdots, 8;\ j = p, q)$. In the present work, a linear fitting method combined with a set of control points is adopted to retrieve the boundary stress coefficients from the in-plane stress boundary conditions in Eq. 20. The Chebyshev–Gauss–Labotto point distribution, due to its non-uniformity and stability, is superior to the uniform point distribution in capturing the local feature of the boundary stress distribution and is thus chosen to be distributed on the boundary edges ($\xi = \pm 1$, $\eta = \pm 1$) of the plate, which are given as

$$\begin{aligned} &\xi = \pm 1: \quad \eta_j = \cos\left(\frac{j-1}{\mathcal{N}_{CGL}^{\eta} - 1}\pi\right) \quad j = 1, 2, \cdots, \mathcal{N}_{CGL}^{\eta} \\ &\eta = \pm 1: \quad \xi_i = \cos\left(\frac{i-1}{\mathcal{N}_{CGL}^{\xi} - 1}\pi\right) \quad i = 1, 2, \cdots, \mathcal{N}_{CGL}^{\xi} \end{aligned} \tag{22}$$

where $\mathcal{N}_{CGL}^{\eta}$ and $\mathcal{N}_{CGL}^{\xi}$ are the number of the Chebyshev–Gauss–Labotto points, which equals to the number of terms in each stress boundary condition of Eq. 20. Substituting the Chebyshev–Gauss–Labotto points into Eq. 20, a set of linear algebraic equations corresponding to each stress boundary condition can be obtained. A detailed process of determining the boundary stress coefficients can be found in Ref. [9]. In particular, for the case of no external forces on four edges (see Eq. 11), all boundary stress coefficients equal to zero, and therefore the stress constraint equations from Eq. 21 can be directly written as

$$
\begin{aligned}
&0=\sum_{p=0}^{P}\phi_{pq}L_p(-1), \quad 0=\sum_{p=0}^{P}\phi_{pq}L_p(1)\\
&0=\sum_{q=0}^{Q}\phi_{pq}L_q(-1), \quad 0=\sum_{q=0}^{Q}\phi_{pq}L_q(1)\\
&0=\sum_{p=1}^{P}\phi_{pq}\frac{\partial L_p(\xi)}{\partial \xi}\Big|_{\xi=-1}, \quad 0=\sum_{p=1}^{P}\phi_{pq}\frac{\partial L_p(\xi)}{\partial \xi}\Big|_{\xi=1}\\
&0=\sum_{q=1}^{Q}\phi_{pq}\frac{\partial L_q(\eta)}{\partial \eta}\Big|_{\eta=-1}, \quad 0=\sum_{q=1}^{Q}\phi_{pq}\frac{\partial L_q(\eta)}{\partial \eta}\Big|_{\eta=1}
\end{aligned} \tag{23}
$$

Furthermore, the stress constraint equations given by Eq. 21 need to be included into the first variation of the thermoelastic complementary energy $\delta\Pi_C$ shown in Eq. 14 by applying the Lagrangian multiplier method, which can be expressed using

$$
\delta\mathbb{L}_{\mathbb{A}}(\phi_{00},\phi_{01},\cdots,\phi_{PQ},\chi_2^1,\chi_3^1,\cdots,\chi_P^8)=\delta\Pi_C(\phi_{00},\phi_{01},\cdots,\phi_{PQ})+\delta\Pi_{LM}^* \tag{24}
$$

with

$$
\begin{aligned}
\Pi_{LM}^* =\ & \frac{4}{b^2}\sum_{q=2}^{Q}\chi_q^1\left(\sum_{p=0}^{P}\phi_{pq}L_p(-1)-\Lambda_q^1\right)+\frac{4}{b^2}\sum_{q=2}^{Q}\chi_q^2\left(\sum_{p=0}^{P}\phi_{pq}L_p(1)-\Lambda_q^2\right)\\
&+\frac{4}{a^2}\sum_{p=2}^{P}\chi_p^3\left(\sum_{q=0}^{Q}\phi_{pq}L_q(-1)-\Lambda_p^3\right)+\frac{4}{a^2}\left(\sum_{p=2}^{P}\chi_p^4\sum_{q=0}^{Q}\phi_{pq}L_q(1)-\Lambda_p^4\right)\\
&-\frac{4}{ab}\sum_{q=1}^{Q}\chi_q^5\left(\sum_{p=1}^{P}\phi_{pq}\frac{\partial L_p(\xi)}{\partial \xi}\Big|_{\xi=-1}-\Lambda_q^5\right)-\frac{4}{ab}\sum_{q=1}^{Q}\chi_q^6\left(\sum_{p=1}^{P}\phi_{pq}\frac{\partial L_p(\xi)}{\partial \xi}\Big|_{\xi=1}-\Lambda_q^6\right)\\
&-\frac{4}{ab}\sum_{p=1}^{P}\chi_p^7\left(\sum_{q=1}^{Q}\phi_{pq}\frac{\partial L_q(\eta)}{\partial \eta}\Big|_{\eta=-1}-\Lambda_p^7\right)-\frac{4}{ab}\sum_{p=1}^{P}\chi_p^8\left(\sum_{q=1}^{Q}\phi_{pq}\frac{\partial L_q(\eta)}{\partial \eta}\Big|_{\eta=1}-\Lambda_p^8\right)
\end{aligned} \tag{25}
$$

where Π_{LM}^* denotes the stress constraint function generated by applying the Lagrangian multiplier method, which is equivalent to the stress boundary condition along the edges of the plate; χ_j^i $(i=1,2,\cdots,8;\ j=p,q\ )$ are the j^{th} Lagrangian multiplier corresponding to the i^{th} stress boundary condition. Substituting Eqs. 14, 18 and 25 into Eq. 24 and setting the first variation of the Lagrangian function $\delta\mathbb{L}_A(\phi_{00},\phi_{01},\cdots,\phi_{PQ},\chi_2^1,\chi_3^1,\cdots,\chi_P^8)$ to zero, that is, [65]

$$\delta \mathbb{L}_{\mathbb{A}}(\phi_{00}, \phi_{01}, \cdots, \phi_{PQ}, \chi_2^1, \chi_3^1, \cdots, \chi_P^8) = 0 \tag{26}$$

a set of linear algebraic equations can be obtained and expressed in the following matrix form:

$$\begin{bmatrix} \mathbf{K} & \mathbf{LM} \\ \mathbf{LM^T} & \mathbf{O} \end{bmatrix} \begin{Bmatrix} \boldsymbol{\phi} \\ \boldsymbol{\chi} \end{Bmatrix} = \begin{Bmatrix} \mathbf{\Psi}^{th} \\ \mathbf{\Lambda} \end{Bmatrix} \tag{27}$$

where $\mathbf{K}$ and $\mathbf{\Psi}^{th}$ are similar to those in Eq. 17, but both of them are obtained based on the Airy's stress function given by Eq. 18; $\mathbf{LM}$ is the Lagrangian multiplier matrix generated by the the first variation of the stress constraint function, that is, $\delta \Pi_{LM}^*$; $\mathbf{LM^T}$ is the transposed form of the Lagrangian multiplier matrix $\mathbf{LM}$; $\mathbf{O}$ is the null matrix; $\boldsymbol{\phi}$ and $\boldsymbol{\chi}$ are the unknown vectors to be determined; $\mathbf{\Lambda}$ is the boundary stress vector, which collects all the boundary stress coefficients Λ_j^i $(i = 1, 2, \cdots, 8;\ j = p, q)$. It is noted that the linear algebraic equations $\mathbf{LM^T}\boldsymbol{\phi} = \mathbf{\Lambda}$ in Eq. 27 are equivalent to the stress constraint equations from Eq. 21. Once the boundary stress coefficients in Eq. 20 are determined by applying the mathematical fitting method, the Legendre polynomial coefficients $\phi_{pq}(p = 0, 1, \cdots, P; q = 0, 1, \cdots, Q)$ can be obtained by using Eq. 27 and thus the in-plane thermoelastic problem of VAT composite plates subjected to a combination of both temperature change and pure stress boundary constraints is solved. In particular, for the case of no external forces on four edges of the plate, Eq. 27 can be reduced to

$$\begin{bmatrix} \mathbf{K} & \mathbf{LM} \\ \mathbf{LM^T} & \mathbf{O} \end{bmatrix} \begin{Bmatrix} \boldsymbol{\phi} \\ \boldsymbol{\chi} \end{Bmatrix} = \begin{Bmatrix} \mathbf{\Psi}^{th} \\ \breve{\mathbf{O}} \end{Bmatrix} \tag{28}$$

where $\breve{\mathbf{O}}$ is the null vector. Note that, for this particular case, the in-plane response of the tow-steered plate is only controlled by temperature change. On the other hand, if no temperature change occurs within the plate domain, that is, $\Delta T(x, y) \equiv 0$, the thermally induced load vector $\mathbf{\Psi}^{th}$ will vanish in Eq. 27 and thus the governing equation given by

Eq. 27 is reduced into

$$\begin{bmatrix} \mathbf{K} & \mathbf{LM} \\ \mathbf{LM^T} & \mathbf{O} \end{bmatrix} \begin{Bmatrix} \boldsymbol{\phi} \\ \boldsymbol{\chi} \end{Bmatrix} = \begin{Bmatrix} \breve{\mathbf{O}} \\ \boldsymbol{\Lambda} \end{Bmatrix} \tag{29}$$

For such a special case, the in-plane response of the tow-steered plate is fully determined by pure stress boundary constraints, which has been studied in details in Ref. [9]. However, from a mathematical point of view, Eq. 27 can be regarded as a linear superposition of Eq. 28 and Eq. 29, which means that the in-plane force resultants of the tow-steered plate obtained under a combination of thermal and mechanical loadings can be regarded as a superposition of those obtained under their respective loadings.

Case B

In this section, the Rayleigh-Ritz formulation is extended to the case of a combination of both temperature change and pure displacement boundary constraint. Without loss of generality, the in-plane displacement boundary conditions along the edges ($\xi = \pm 1$, $\eta = \pm 1$) of the plate can be expressed in the following form:

$$\begin{aligned} \xi = -1 : &\begin{cases} u^0 = \widetilde{u}_1^0(\eta) \\ v^0 = \widetilde{v}_1^0(\eta) \end{cases}; \quad \xi = 1 : \begin{cases} u^0 = \widetilde{u}_2^0(\eta) \\ v^0 = \widetilde{v}_2^0(\eta) \end{cases} \\ \eta = -1 : &\begin{cases} u^0 = \widetilde{u}_3^0(\xi) \\ v^0 = \widetilde{v}_3^0(\xi) \end{cases}; \quad \eta = 1 : \begin{cases} u^0 = \widetilde{u}_4^0(\xi) \\ v^0 = \widetilde{v}_4^0(\xi) \end{cases} \end{aligned} \tag{30}$$

where $\widetilde{u}_i^0$ and $\widetilde{v}_i^0$ ($i = 1, 2, 3, 4$) are the prescribed in-plane displacements along the i^{th} boundary edge of the plate. As the boundary conditions on four edges are specified solely in terms of displacements, there exists no stress boundary constraints along the edges of the plate. As such, the stress constraint function Π_{LM}^* in Eq. 25 obtained by applying the Lagrangian multiplier method is unnecessary. However, the displacement boundary constraints on four edges of the plate require to be satisfied in boundary integral form and given by [9]

$$
\begin{aligned}
\Pi_D^* =& \frac{2}{b}\int_{-1}^{1}\left[\frac{\partial^2\Phi}{\partial\eta^2}\widetilde{u}_1^0\right]_{\xi=-1}\mathrm{d}\eta - \frac{2}{a}\int_{-1}^{1}\left[\frac{\partial^2\Phi}{\partial\xi\partial\eta}\widetilde{v}_1^0\right]_{\xi=-1}\mathrm{d}\eta + \\
& \frac{2}{b}\int_{-1}^{1}\left[\frac{\partial^2\Phi}{\partial\eta^2}\widetilde{u}_2^0\right]_{\xi=1}\mathrm{d}\eta - \frac{2}{a}\int_{-1}^{1}\left[\frac{\partial^2\Phi}{\partial\xi\partial\eta}\widetilde{v}_2^0\right]_{\xi=1}\mathrm{d}\eta - \\
& \frac{2}{b}\int_{-1}^{1}\left[\frac{\partial^2\Phi}{\partial\xi\partial\eta}\widetilde{u}_3^0\right]_{\eta=-1}\mathrm{d}\xi + \frac{2}{a}\int_{-1}^{1}\left[\frac{\partial^2\Phi}{\partial\xi^2}\widetilde{v}_3^0\right]_{\eta=-1}\mathrm{d}\xi - \\
& \frac{2}{b}\int_{-1}^{1}\left[\frac{\partial^2\Phi}{\partial\xi\partial\eta}\widetilde{u}_4^0\right]_{\eta=1}\mathrm{d}\xi + \frac{2}{a}\int_{-1}^{1}\left[\frac{\partial^2\Phi}{\partial\xi^2}\widetilde{v}_4^0\right]_{\eta=1}\mathrm{d}\xi
\end{aligned}
\tag{31}
$$

where Π_D^* denotes the displacement constraint function representing the work done by the unknown force along the applied boundary displacement. Furthermore, the first variation of the displacement constraint function $\delta\Pi_D^*$ need to be included into the first variation of the thermoelastic complementary energy $\delta\Pi_C$ in Eq. 14, that is,

$$
\delta\Pi_{Tot}(\phi_{00}, \phi_{01}, \cdots, \phi_{PQ}) = \delta\Pi_C(\phi_{00}, \phi_{01}, \cdots, \phi_{PQ}) + \delta\Pi_D^*(\phi_{00}, \phi_{01}, \cdots, \phi_{PQ}) \tag{32}
$$

By substituting Eqs. 14 and 31 into Eq. 32 and setting the first variation of the total thermoelastic complementary energy $\delta\Pi_{Tot}(\phi_{00}, \phi_{01}, \cdots, \phi_{PQ})$ to 0, that is,

$$
\delta\Pi_{Tot}(\phi_{00}, \phi_{01}, \cdots, \phi_{PQ}) = 0 \tag{33}
$$

a set of linear algebraic equations is then generated and expressed in the following matrix form:

$$
\mathbf{K}\boldsymbol{\phi} = \boldsymbol{\Psi}^{dis} + \boldsymbol{\Psi}^{th} \tag{34}
$$

where $\mathbf{K}$ and $\boldsymbol{\Psi}^{th}$ are similar to those in Case A; $\boldsymbol{\Psi}^{dis}$ is the load vector induced by the prescribed displacement along the boundary edges of the plate, which is obtained from Eq. 31. In particular, if the in-plane displacements on four edges of the plate are fully constrained, that is, $\widetilde{u}_i^0 = \widetilde{v}_i^0 = 0$ $(i = 1, 2, 3, 4)$, the displacement-induced load vector $\boldsymbol{\Psi}^{dis}$ will vanish in Eq. 34 and thus the resulting equation given by Eq. 34 has a form similar to that in Eq. 17. For such a particular case, the in-plane behaviour of the plate is only driven by the thermal loadings. The robustness and effectiveness of the proposed Rayleigh-Ritz model for this particular case will be demonstrated in Section. 4. On the other hand, if there exists no temperature change within the plate, that is, $\Delta T(x, y) \equiv 0$, the thermally induced load vector $\mathbf{\Psi}^{th}$ will vanish in Eq. 34 and the governing equation is expressed as

$$\mathbf{K}\boldsymbol{\phi} = \mathbf{\Psi}^{dis} \tag{35}$$

For this case, the in-plane response of the panel is dominated by the pure displacement boundary constraints, which has been studied in details in Ref. [9].

Case C

In this part, a more general situation where there simultaneously exists both in-plane stress and displacement boundary conditions is considered. The panel is assumed to be exposed to a combination of both temperature change and mixed in-plane boundary constraints. As in the case of pure stress boundary constraints, the Rayleigh-Ritz formulation enhanced by the Lagrangian multiplier method continues to be employed. However, both the stress constraint function Π^*_{LM} and displacement constraint function Π^*_D need to be included into the first variation of the thermoelastic complementary energy $\delta\Pi_C$, that is:

$$\delta\mathbb{L}_B(\phi_{00}, \phi_{01}, \cdots, \phi_{PQ}, \chi^1_2, \chi^1_3, \cdots, \chi^8_P) = \delta\Pi_C + \delta\Pi^*_{LM} + \delta\Pi^*_D \tag{36}$$

Substituting Eqs. 14, 25 and 31 into Eq. 36 and setting the first variation of the Lagrangian function $\delta\mathbb{L}_B(\phi_{00}, \phi_{01}, \cdots, \phi_{PQ}, \chi^1_2, \chi^1_3, \cdots, \chi^8_P)$ to zero, that is,

$$\delta\mathbb{L}_B(\phi_{00}, \phi_{01}, \cdots, \phi_{PQ}, \chi^1_2, \chi^1_3, \cdots, \chi^8_P) = 0 \tag{37}$$

a set of linear algebraic equations, which governs the in-plane thermoelastic problem of the VAT plate subjected to a combination of both temperature change and mixed in-plane boundary constraints, can be obtained and expressed in the following matrix form:

$$\begin{bmatrix} \mathbf{K} & \mathbf{LM} \\ \mathbf{LM^T} & \mathbf{O} \end{bmatrix} \begin{Bmatrix} \boldsymbol{\phi} \\ \boldsymbol{\chi} \end{Bmatrix} = \begin{Bmatrix} \mathbf{\Psi}^{dis} + \mathbf{\Psi}^{th} \\ \mathbf{\Lambda} \end{Bmatrix} \tag{38}$$

where $\mathbf{K}$ and $\mathbf{\Psi}^{th}$ are similar to those in Case A, while $\mathbf{\Psi}^{dis}$ is the same as that in Case B. However, it is noted that the in-plane stress and displacement boundary constraints in the same direction (ξ or η) of each panel edge are conjugate, which indicates that if the in-plane displacement boundary constraint in that direction of the panel edge is activated, the conjugate stress constraint tends to be suppressed, and vice versa. From this point of view, there exists two special cases of governing equation. For example, when the in-plane stress boundary constraints are applied on all four edges of the panel, the corresponding displacement boundary constraints remain dormant and thus the first variation of the displacement constraint function $\delta\Pi_D^*$ needs to be removed from Eq. 36. For this case, the governing equation given by Eq. 38 is reduced into that in Eq. 27. On the other hand, when the in-plane displacement boundary constraints are imposed on all four edges of the panel, the corresponding stress boundary constraints are suppressed and thus the first variation of the stress constraint function $\delta\Pi_{LM}^*$ needs to be removed from Eq. 36. Under such circumstance, the governing equation given by Eq. 38 is reduced into that in Eq. 34. However, in most cases, there appears mixed boundary constraints on the boundary edges of the plate. For example, the plate in thermal environment is assumed to be subjected to uniform end-shortening with transverse edges free to deform, which has been extensively studied in previous researches [1, 3, 7, 9]. This is a mixed in-plane boundary condition and given by

$$\begin{aligned} x = \pm a/2: &\quad u^0(\pm a/2, y) = \mp\Delta_x; &\quad N_{xy}^0(\pm a/2, y) = 0 \\ y = \pm b/2: &\quad N_y^0(x, \pm b/2) = 0; &\quad N_{yx}^0(x, \pm b/2) = 0 \end{aligned} \tag{39}$$

For this case, the boundary stress coefficients related to prescribed stress boundary conditions equal to zero, that is,

$$\begin{aligned} &0 = \sum_{q=0}^{Q} \phi_{pq} L_q(-1), \quad 0 = \sum_{q=0}^{Q} \phi_{pq} L_q(1) \\ &0 = \sum_{p=1}^{P} \phi_{pq} \frac{\partial L_p(\xi)}{\partial \xi}\Big|_{\xi=-1}, \quad 0 = \sum_{p=1}^{P} \phi_{pq} \frac{\partial L_p(\xi)}{\partial \xi}\Big|_{\xi=1} \\ &0 = \sum_{q=1}^{Q} \phi_{pq} \frac{\partial L_q(\eta)}{\partial \eta}\Big|_{\eta=-1}, \quad 0 = \sum_{q=1}^{Q} \phi_{pq} \frac{\partial L_q(\eta)}{\partial \eta}\Big|_{\eta=1} \end{aligned} \tag{40}$$

As such, the stress constraint function Π_{LM}^* given by Eq. 25 can be simplified as

$$\begin{aligned}\Pi_{LM}^* = & \frac{4}{a^2}\sum_{p=2}^{P}\chi_p^3\sum_{q=0}^{Q}\phi_{pq}L_q(-1) + \frac{4}{a^2}\sum_{p=2}^{P}\chi_p^4\sum_{q=0}^{Q}\phi_{pq}L_q(1) \\ & - \frac{4}{ab}\sum_{q=1}^{Q}\chi_q^5\sum_{p=1}^{P}\phi_{pq}\frac{\partial L_p(\xi)}{\partial \xi}\Big|_{\xi=-1} - \frac{4}{ab}\sum_{q=1}^{Q}\chi_q^6\sum_{p=1}^{P}\phi_{pq}\frac{\partial L_p(\xi)}{\partial \xi}\Big|_{\xi=1} \\ & - \frac{4}{ab}\sum_{p=1}^{P}\chi_p^7\sum_{q=1}^{Q}\phi_{pq}\frac{\partial L_q(\eta)}{\partial \eta}\Big|_{\eta=-1} - \frac{4}{ab}\sum_{p=1}^{P}\chi_p^8\sum_{q=1}^{Q}\phi_{pq}\frac{\partial L_q(\eta)}{\partial \eta}\Big|_{\eta=1}\end{aligned} \tag{41}$$

Moreover, the displacement constraint function Π_D^* given by Eq. 31 can be degenerated into

$$\Pi_D^* = -\int_{-1}^{1}\frac{2}{b}\frac{\partial^2\Phi}{\partial\eta^2}\Delta_x \mathrm{d}\eta - \int_{-1}^{1}\frac{2}{b}\frac{\partial^2\Phi}{\partial\eta^2}\Delta_x \mathrm{d}\eta \tag{42}$$

Finally, the governing equation given by Eq. 38 is reduced into

$$\begin{bmatrix}\mathbf{K} & \mathbf{LM} \\ \mathbf{LM^T} & \mathbf{O}\end{bmatrix}\begin{Bmatrix}\boldsymbol{\phi} \\ \boldsymbol{\chi}\end{Bmatrix} = \begin{Bmatrix}\boldsymbol{\Psi}^{dis} + \boldsymbol{\Psi}^{th} \\ \breve{\mathbf{O}}\end{Bmatrix} \tag{43}$$

In particular, if the in-plane longitudinal displacement on the edges ($x = \pm a/2$) of the plate are fully constrained, that is, $\Delta_x = 0$, the displacement-induced load vector $\boldsymbol{\Psi}^{dis}$ will vanish in Eq. 43. Under such circumstance, the in-plane behaviour of the plate is only controlled by the temperature rise or drop. On the other hand, if there exists no temperature change within the plate, that is, $\Delta T(x, y) \equiv 0$, the thermally induced load vector $\boldsymbol{\Psi}^{th}$ will vanish in Eq. 43. In such case, the governing equation given by Eq. 43 is then reduced to Eq. 44 and the in-plane response of the plate is driven by uniform end-shortening, which has been studied in details in Ref. [9].

$$\begin{bmatrix}\mathbf{K} & \mathbf{LM} \\ \mathbf{LM^T} & \mathbf{O}\end{bmatrix}\begin{Bmatrix}\boldsymbol{\phi} \\ \boldsymbol{\chi}\end{Bmatrix} = \begin{Bmatrix}\boldsymbol{\Psi}^{dis} \\ \breve{\mathbf{O}}\end{Bmatrix} \tag{44}$$

It is noted that for all the cases above, only the assumption of mid-plane symmetry is applied on the VAT composite plate, as described before. Therefore, this proposed Rayleigh-Ritz model is suitable to a more general layup configuration, even with extension-shear coupling, that is, $A_{16} \neq 0$ and $A_{26} \neq 0$.

3.3. Thermomechanical buckling analysis

In this section, the thermomechanical buckling analysis of VAT composite plates under the non-uniform in-plane force resultants (N_x^0, N_y^0 and N_{xy}^0) obtained by the previous in-plane thermoelastic analysis is performed by employing the Rayleigh-Ritz method. In the present work, the governing equation of thermomechanical buckling problem is derived based on the third-order shear deformation theory of Reddy's type, which has been extensively employed for thermal or mechanical buckling analysis [66, 67, 28, 68]. The in-plane displacement fields (u and v) and the out-of-plane displacement field (w) of the plate in its buckled state can be expressed as [58]:

$$\begin{aligned} u(x,y,z) &= u^0 + z\phi_x^0(x,y) - \frac{4}{3h^2}z^3\left(\phi_x^0 + \frac{\partial w^0}{\partial x}\right) \\ v(x,y,z) &= v^0 + z\phi_y^0(x,y) - \frac{4}{3h^2}z^3\left(\phi_y^0 + \frac{\partial w^0}{\partial y}\right) \\ w(x,y,z) &= w^0(x,y) \end{aligned} \tag{45}$$

where ϕ_x^0 and ϕ_y^0 are the independent rotations of the normal to the middle surface about the y and x axis, respectively; u^0, v^0 and w^0 is the in-plane and out-of-plane displacements of the middle surface, respectively. Herein, the in-plane displacement fields of the panel induced by the deflection and rotation of the middle surface are considered. As such, the strain–displacement relationship of the plate in the linear regime can be written as [58]:

$$\begin{aligned} \boldsymbol{\epsilon} &= \begin{Bmatrix} \varepsilon_x & \varepsilon_y & \gamma_{xy} \end{Bmatrix}^{\mathrm{T}} = z\boldsymbol{\epsilon}^{(1)} + z^3\boldsymbol{\epsilon}^{(3)} \\ \boldsymbol{\gamma} &= \begin{Bmatrix} \gamma_{yz} & \gamma_{xz} \end{Bmatrix}^{\mathrm{T}} = \boldsymbol{\gamma}^{(0)} + z^2\boldsymbol{\gamma}^{(2)} \end{aligned} \tag{46}$$

with ($c_2 = 3c_1$ and $c_1 = 4/3h^2$)

$$\boldsymbol{\epsilon}^{(1)} = \begin{Bmatrix} \varepsilon_x^{(1)} & \varepsilon_y^{(1)} & \gamma_{xy}^{(1)} \end{Bmatrix}^{\mathrm{T}} = \begin{Bmatrix} \frac{\partial \phi_x^0}{\partial x} \\ \frac{\partial \phi_y^0}{\partial y} \\ \frac{\partial \phi_x^0}{\partial y} + \frac{\partial \phi_y^0}{\partial x} \end{Bmatrix} \tag{47a}$$

$$\boldsymbol{\epsilon}^{(3)} = \begin{Bmatrix} \varepsilon_x^{(3)} & \varepsilon_y^{(3)} & \gamma_{xy}^{(3)} \end{Bmatrix}^{\mathrm{T}} = -c_1 \begin{Bmatrix} \frac{\partial \phi_x^0}{\partial x} + \frac{\partial^2 w^0}{\partial x^2} \\ \frac{\partial \phi_y^0}{\partial y} + \frac{\partial^2 w^0}{\partial y^2} \\ \frac{\partial \phi_x^0}{\partial y} + \frac{\partial \phi_y^0}{\partial x} + 2\frac{\partial^2 w^0}{\partial x \partial y} \end{Bmatrix} \tag{47b}$$

$$\boldsymbol{\gamma}^{(0)} = \left\{\gamma_{yz}^{(0)} \quad \gamma_{xz}^{(0)}\right\}^{\mathrm{T}} = \left\{\begin{matrix} \phi_y^0 + \frac{\partial w^0}{\partial y} \\ \phi_x^0 + \frac{\partial w^0}{\partial x} \end{matrix}\right\} \tag{47c}$$

$$\boldsymbol{\gamma}^{(2)} = \left\{\gamma_{yz}^{(2)} \quad \gamma_{xz}^{(2)}\right\}^{\mathrm{T}} = -c_2 \left\{\begin{matrix} \phi_y^0 + \frac{\partial w^0}{\partial y} \\ \phi_x^0 + \frac{\partial w^0}{\partial x} \end{matrix}\right\} \tag{47d}$$

The constitutive equation of the VAT composite pate is given as in the following matrix form

$$\left\{\begin{matrix} \mathbf{M} \\ \mathbf{P} \end{matrix}\right\} = \begin{bmatrix} \mathbf{D} & \mathbf{F} \\ \mathbf{F} & \mathbf{H} \end{bmatrix} \left\{\begin{matrix} \boldsymbol{\epsilon}^{(\mathbf{1})} \\ \boldsymbol{\epsilon}^{(\mathbf{3})} \end{matrix}\right\} - \left\{\begin{matrix} \mathbf{M}^{th} \\ \mathbf{P}^{th} \end{matrix}\right\} \tag{48a}$$

$$\left\{\begin{matrix} \mathbf{Q} \\ \mathbf{R} \end{matrix}\right\} = \begin{bmatrix} \mathbf{A} & \mathbf{D} \\ \mathbf{D} & \mathbf{F} \end{bmatrix} \left\{\begin{matrix} \boldsymbol{\gamma}^{(\mathbf{0})} \\ \boldsymbol{\gamma}^{(\mathbf{2})} \end{matrix}\right\} \tag{48b}$$

with

$$(A_{ij}, B_{ij}, D_{ij}, E_{ij}, F_{ij}, H_{ij}) = \sum_{k=0}^{K} \int_{z_{k-1}}^{z_k} Q_{ij}^k(x,y)(1, z, z^2, z^3, z^4, z^6)\mathrm{d}z \tag{49a}$$

$$(A_{ij}, D_{ij}, F_{ij},) = \sum_{k=0}^{K} \int_{z_{k-1}}^{z_k} Q_{ij}^k(x,y)(1, z^2, z^4)\mathrm{d}z \tag{49b}$$

where the stiffnesses in Eq. 49a are defined for $i, j = 1, 2, 6$ and those in Eq. 49b are defined for $i, j = 4, 5$. The thermal moment resultant vectors $\mathbf{M}^{th}$ and $\mathbf{P}^{th}$ are expressed as

$$\mathbf{M}^{th} = \left\{\begin{matrix} M_x^{th} \\ M_y^{th} \\ M_{xy}^{th} \end{matrix}\right\} = \sum_{k=0}^{K} \int_{z_{k-1}}^{z_k} \begin{bmatrix} Q_{11}^k(x,y) & Q_{12}^k(x,y) & Q_{16}^k(x,y) \\ Q_{12}^k(x,y) & Q_{22}^k(x,y) & Q_{26}^k(x,y) \\ Q_{16}^k(x,y) & Q_{26}^k(x,y) & Q_{66}^k(x,y) \end{bmatrix} \left\{\begin{matrix} \alpha_x^k(x,y)\Delta T \\ \alpha_y^k(x,y)\Delta T \\ \alpha_{xy}^k(x,y)\Delta T \end{matrix}\right\} z\mathrm{d}z \tag{50a}$$

$$\mathbf{P}^{th}=\begin{Bmatrix}P_x^{th}\\P_y^{th}\\P_{xy}^{th}\end{Bmatrix}=\sum_{k=0}^{K}\int_{z_{k-1}}^{z_k}\begin{bmatrix}Q_{11}^k(x,y) & Q_{12}^k(x,y) & Q_{16}^k(x,y)\\Q_{12}^k(x,y) & Q_{22}^k(x,y) & Q_{26}^k(x,y)\\Q_{16}^k(x,y) & Q_{26}^k(x,y) & Q_{66}^k(x,y)\end{bmatrix}\begin{Bmatrix}\alpha_x^k(x,y)\Delta T\\\alpha_y^k(x,y)\Delta T\\\alpha_{xy}^k(x,y)\Delta T\end{Bmatrix}z^3\mathrm{d}z \quad (50b)$$

It is noted that for symmetric layups, all three components of the vector $\mathbf{M}^{th}$ or $\mathbf{P}^{th}$ are zero and thus will vanish in the constitutive equation given by Eq. 48a.

The total potential energy of the VAT composite plate in its buckled shape can be expressed as in condensed form:

$$\Pi = U_b + U_s + V \quad (51)$$

in which

$$U_b=\frac{1}{2}\iint_{\Omega}\left[M_x^0\varepsilon_x^{(1)}+M_y^0\varepsilon_y^{(1)}+M_{xy}^0\gamma_{xy}^{(1)}+P_x^0\varepsilon_x^{(3)}+P_y^0\varepsilon_y^{(3)}+P_{xy}^0\gamma_{xy}^{(3)}\right]\mathrm{d}x\mathrm{d}y \quad (52a)$$

$$U_s=\frac{1}{2}\iint_{\Omega}\left[Q_{yz}^0\gamma_{yz}^{(0)}+Q_{xz}^0\gamma_{yz}^{(0)}+R_{yz}^0\gamma_{xz}^{(2)}+R_{xz}^0\gamma_{xz}^{(2)}\right]\mathrm{d}x\mathrm{d}y \quad (52b)$$

$$V=\frac{1}{2}\iint_{\Omega}\left[N_x^0\left(\frac{\partial w^0}{\partial x}\right)^2+N_y^0\left(\frac{\partial w^0}{\partial y}\right)^2+N_{xy}^0\frac{\partial w^0}{\partial x}\frac{\partial w^0}{\partial y}\right]\mathrm{d}x\mathrm{d}y \quad (52c)$$

where U_b and U_s are the bending and shear strain energies of the plate in its buckled state, respectively; V is the external work of the plate done by the non-uniform in-plane force resultants (N_x^0, N_y^0 and N_{xy}^0). Note that, the above expressions need to be converted into a non-dimensional form for analysis.

The Rayleigh-Ritz method is then adopted to solve the buckling problem of the VAT plate under a combination of thermal and mechanical loads. Because the analytical modelling is derived from a weak form formula, only the essential or geometrical boundary conditions need to be satisfied. As such, the out-of-plane boundary constraints in terms of displacements will be applied on the edges of the panel. For the panel with four edges clamped, the out-of-plane boundary conditions are given by:

$$
\begin{aligned}
&\xi = -1 : \begin{cases} w^0(-1,\eta) = 0 \\ \phi_x^0(-1,\eta) = 0 \\ \phi_y^0(-1,\eta) = 0 \end{cases} ; \quad \xi = 1 : \begin{cases} w^0(1,\eta) = 0 \\ \phi_x^0(1,\eta) = 0 \\ \phi_y^0(1,\eta) = 0 \end{cases} \\
&\eta = -1 : \begin{cases} w^0(\xi,-1) = 0 \\ \phi_x^0(\xi,-1) = 0 \\ \phi_y^0(\xi,-1) = 0 \end{cases} ; \quad \eta = 1 : \begin{cases} w^0(\xi,1) = 0 \\ \phi_x^0(\xi,1) = 0 \\ \phi_y^0(\xi,1) = 0 \end{cases}
\end{aligned} \tag{53}
$$

For the panel with four edges simply supported, the out-of-plane boundary conditions can be expressed as:

$$
\begin{aligned}
&\xi = -1 : \begin{cases} w^0(-1,\eta) = 0 \\ \phi_y^0(-1,\eta) = 0 \end{cases} ; \quad \xi = 1 : \begin{cases} w^0(1,\eta) = 0 \\ \phi_y^0(1,\eta) = 0 \end{cases} \\
&\eta = -1 : \begin{cases} w^0(\xi,-1) = 0 \\ \phi_x^0(\xi,-1) = 0 \end{cases} ; \quad \eta = 1 : \begin{cases} w^0(\xi,1) = 0 \\ \phi_x^0(\xi,1) = 0 \end{cases}
\end{aligned} \tag{54}
$$

Herein, the displacement w^0 and rotations ϕ_x^0 and ϕ_y^0 used for the buckling analysis can be constructed by Legendre polynomials multiplying with functions that satisfy essential or geometrical boundary conditions along four edges of the panel. For the panel with four edges clamped, the displacement fields can be written as:

$$
\begin{aligned}
w^0(\xi,\eta) &= (1-\xi^2)(1-\eta^2)\sum_{m=0}^{M}\sum_{n=0}^{N}\mathcal{A}_{mn}L_m(\xi)L_n(\eta) \\
\phi_x^0(\xi,\eta) &= (1-\xi^2)(1-\eta^2)\sum_{r=0}^{R}\sum_{s=0}^{S}\mathcal{B}_{rs}L_r(\xi)L_s(\eta) \\
\phi_y^0(\xi,\eta) &= (1-\xi^2)(1-\eta^2)\sum_{g=0}^{G}\sum_{h=0}^{H}\mathcal{C}_{gh}L_g(\xi)L_h(\eta)
\end{aligned} \tag{55}
$$

For the panel with four edges simply supported, the displacement fields can be written as:

$$
\begin{aligned}
w^0(\xi,\eta) &= (1-\xi^2)(1-\eta^2)\sum_{m=0}^{M}\sum_{n=0}^{N}\mathcal{A}_{mn}L_m(\xi)L_n(\eta)\\
\phi_x^0(\xi,\eta) &= (1-\eta^2)\sum_{r=0}^{R}\sum_{s=0}^{S}\mathcal{B}_{rs}L_r(\xi)L_s(\eta)\\
\phi_y^0(\xi,\eta) &= (1-\xi^2)\sum_{g=0}^{G}\sum_{h=0}^{H}\mathcal{C}_{gh}L_g(\xi)L_h(\eta)
\end{aligned}
\tag{56}
$$

where $\mathcal{A}_{mn}$, $\mathcal{B}_{rs}$ and $\mathcal{C}_{gh}$ are the polynomial coefficients of the displacement fields w^0, ϕ_x^0 and ϕ_y^0, respectively. Other boundary conditions can be dealt with in a similar way. Substituting Eqs. 48, 52 and 55 or 56 into Eq. 51 and minimizing the total potential energy Π with respect to $\mathcal{A}_{mn}(m=0,1,\cdots,M;n=0,1,\cdots,N)$, $\mathcal{B}_{rs}(r=0,1,\cdots,R;s=0,1,\cdots,S)$, $\mathcal{C}_{gh}(g=0,1,\cdots,G;h=0,1,\cdots,H)$, that is,

$$
\frac{\partial\Pi}{\partial\mathcal{A}_{mn}}=0;\quad \frac{\partial\Pi}{\partial\mathcal{B}_{rs}}=0;\quad \frac{\partial\Pi}{\partial\mathcal{C}_{gh}}=0 \tag{57}
$$

a set of algebraic equations is then obtained and expressed in the following matrix form:

$$
\left(\begin{bmatrix}\mathbf{K}_{11} & \mathbf{K}_{12} & \mathbf{K}_{13}\\ \mathbf{K}_{12} & \mathbf{K}_{22} & \mathbf{K}_{23}\\ \mathbf{K}_{13} & \mathbf{K}_{23} & \mathbf{K}_{33}\end{bmatrix} + \lambda\begin{bmatrix}\mathbf{L}_{11} & \mathbf{0} & \mathbf{0}\\ \mathbf{0} & \mathbf{0} & \mathbf{0}\\ \mathbf{0} & \mathbf{0} & \mathbf{0}\end{bmatrix}\right)\begin{Bmatrix}\mathcal{A}\\ \mathcal{B}\\ \mathcal{C}\end{Bmatrix} = \begin{Bmatrix}\mathbf{0}\\ \mathbf{0}\\ \mathbf{0}\end{Bmatrix} \tag{58}
$$

where $\mathbf{K}_{ij}$ $(i,j=1,2,3)$ is the stiffness matrix of the panel; $\mathbf{L}_{11}$ is the stability matrix due to the in-plane force resultant distribution obtained under a combination of thermal and mechanical loadings; λ is the eigenvalue; $\{\mathcal{A}\quad\mathcal{B}\quad\mathcal{C}\}^{\mathbf{T}}$ is the vector of unknown coefficients corresponding to the shape functions. The detailed expressions of the elements in the matrices are presented in the Appendix. The buckling load and the corresponding mode shape of the VAT plate under a combination of thermal and mechanical loads can then be obtained by solving the eigenvalue equation given by Eq. 58. However, the in-plane force resultants of the tow-steered plate obtained under a combination of thermal and mechanical loadings can be regarded as a superposition of those obtained under their respective loadings. In view of this, Eq. 58 can be divided into:

$$\left(\begin{bmatrix}\mathbf{K}_{11} & \mathbf{K}_{12} & \mathbf{K}_{13}\\ \mathbf{K}_{12} & \mathbf{K}_{22} & \mathbf{K}_{23}\\ \mathbf{K}_{13} & \mathbf{K}_{23} & \mathbf{K}_{33}\end{bmatrix} + \lambda^{(1)}\begin{bmatrix}\mathbf{L}_{11}^{(1)} & \mathbf{0} & \mathbf{0}\\ \mathbf{0} & \mathbf{0} & \mathbf{0}\\ \mathbf{0} & \mathbf{0} & \mathbf{0}\end{bmatrix} + \lambda^{(2)}\begin{bmatrix}\mathbf{L}_{11}^{(2)} & \mathbf{0} & \mathbf{0}\\ \mathbf{0} & \mathbf{0} & \mathbf{0}\\ \mathbf{0} & \mathbf{0} & \mathbf{0}\end{bmatrix}\right)\begin{Bmatrix}\mathcal{A}\\ \mathcal{B}\\ \mathcal{C}\end{Bmatrix} = \begin{Bmatrix}\mathbf{0}\\ \mathbf{0}\\ \mathbf{0}\end{Bmatrix} \tag{59}$$

where $\mathbf{L}_{11}^{(1)}$ and $\mathbf{L}_{11}^{(2)}$ are the stability matrices obtained under the unit thermal and unit mechanical loadings, respectively; $\lambda^{(1)}$ is the temperature difference, while $\lambda^{(2)}$ is the mechanical load multiplier when critical buckling occurs.

4. Results and discussion

This section presents a detailed investigation on both prebuckling and buckling behaviours of VAT composite plates under a combination of both temperature change and general in-plane boundary constraint. Firstly, a comparsion study is carried out to validate the accuracy of the proposed novel Rayleigh-Ritz model. Afterwards, the generalized Rayleigh-Ritz formulation is extended to discuss the effects of fibre orientation angle, temperature change and in-plane boundary constraint on both thermal and thermalmechanical buckling response of the plate. The mechanism of applying tow-steered technology to improve the thermo-mechanical buckling resistance of composite plates is also explored. In order to validate both prebuckling and buckling results obtained by the present Rayleigh-Ritz model, FE modelling of the plate was also carried out using ABAQUS (6.12-1 version). The S4R element was chosen to discretize the panel structure and very fine meshes (60×60) were selected to achieve the desired accuracy. Each finite element was assumed to have a constant fibre orientation for each lamina to model the linear fibre angle distribution. In addition, a subroutine was developed to generate the composite element with independent fibre orientations. Note that, the thickness variation within the tow-steered plate due to tow overlap or gaps were not considered and thus the ply-thickness was regarded as a constant in the present work.

4.1. Model validation and boundary effects

This section firstly conducted a detailed study for the model validation on the in-plane thermoelastic behaviour of VAT composite plates under a combination of both temperature change and general in-plane boundary constraint. In this case, a square plate ($a = b = 150$mm) made of Kevlar/Epoxy material is considered and a four-layer symmetric-balanced layup configuration with linear variation of fibre orientation angle is used. Note, the chosen layup configuration, that is, $[\pm\langle 66.05|11.73\rangle]_s$, is the optimal result for the Kevlar/Epoxy composite material according to the optimization performed by Duran et al. [50, 51]. The ply thickness is 0.254 mm and thus the plate total thickness is $h = 1.016$ mm. The material properties of each lamina are presented in Table. 3, that is, $E_{11} = 80$GPa, $E_{22} = 5.5$GPa, $G_{12} = 2.2$GPa and $v_{12} = 0.34$ with the thermal expansion coefficients $\alpha_1 = -2.0 \times 10^{-6}/°$C and $\alpha_2 = 60 \times 10^{-6}/°$C. The plate studied herein is exposed to a unit uniform temperature change, that is, $\Delta T = 1°$C. On the other hand, six different in-plane boundary constraints, as shown in Fig. 2, are imposed on the edges of the plate, that is, Type-A, Type-B, Type-C,Type-D, Type-E and Type-F, which are described as follows:

- Type-A: all four edges free of external forces;
- Type-B: all four edges fixed against both in-plane normal and tangential displacements;
- Type-C: all four edges restrained against in-plane normal displacements but free to move tangentially;
- Type-D: uniform end shortening in the longitudinal direction with two transverse edges restrained against normal expansion;
- Type-E: two longitudinal edges restrained against normal expansion with two transverse edges free to deform;
- Type-F: uniform end shortening in the longitudinal direction with two transverse edges free to deform.

Type-A belongs to the case of pure stress boundary constraint, while Type-B belongs to the case of pure displacement boundary constraint. Others belong to the case of mixed stress and displacement boundary constraint. The distributions of in-plane force resultants (N_x^0, N_y^0 and N_{xy}^0) of the plate for different combinations of temperature change and in-plane boundary constraint obtained using the present Rayleigh-Ritz method and FE method are shown in Figs. 3-8 and a good agreement between the present results and FE solutions is reached, which approves that the proposed Rayleigh-Ritz model can accurately predict the in-plane thermoelastic behaviour of VAT composite plates, even under a more general in-plane boundary constraint. It is noted that for both Type-C and Type-D boundary constraints, the longitudinal force resultant N_x^0 are constant over the entire plane, while the in-plane shear force resultant N_{xy}^0 are zero, and therefore both of them are not illustrated in Figs. 5 and 6.

From Figs. 3-8, it is observed that for different in-plane boundary constraints, the plate undergoing a unit uniform temperature rise always exhibits a significant difference in the distribution of in-plane force resultant over the panel domain, which indicates that the in-plane boundary constraint has a certain influence on the in-plane thermoelastic behaviour of variable stiffness composite panels. In particular, as shown in Fig. 3, even for the case of no external forces (Type-A), the tow-steered plate still exhibits a highly non-uniform distribution of in-plane residual stresses over the entire plane, which is quite different from that of the straight-fibre plate. For the straight-fibre format, the values of the material properties, namely, the transformed reduced stiffnesses and thermal expansion coefficients, remain unchanged over the plate domain [57] and thus the plate free of external forces will expand or contract uniformly when temperature rises or drops. As such, the in-plane total displacement at arbitrary point of the reference surface is exactly equal to the displacement induced by the free thermal strains and thus no residual stresses develop within the straight-fibre plate that is free of external forces. For VAT layups, however, both material reduced stiffnesses and thermal expansion coefficients are the function of x and y, and thus the plate inevitably suffers from nonuniform residual stresses even if subjected to uniform temperature change, as shown in Fig. 3. These results indicate that non-negligible in-plane residual stresses will appear when tow-steered plates free of external forces are cooled from high curing temperature to room temperature or aerodynamically heated from room temperature to high working temperature.

For the case of fully constrained boundary constraint (Type-B), if the straight-fibre format is considered, the in-plane total strains at arbitrary point of the reference surface are equal to zero [19], which means that each element of material within the plate is fully constrained and thus the in-plane residual stresses are primarily caused by the thermal strains. In so doing, the in-plane force resultants (N_x^0, N_y^0 and N_{xy}^0) within the plate can be explicitly written in terms of the thermal force resultants (N_x^{th}, N_y^{th} and N_{xy}^{th}) as follows

[19]:

$$N_x^0 = -N_x^{th}, \quad N_y^0 = -N_y^{th}, \quad N_{xy}^0 = -N_{xy}^{th} \tag{60}$$

However, this is not the case for VAT layup configurations. Even though both the in-plane normal and tangential strains on all four edges are zero, variable stiffness properties inherent in VAT composite plates, in general, lead to the non-zero total strains on the reference surface, and therefore the mechanical strains are not everywhere equal to the thermal strains over the entire plane, which means that the in-plane force resultants of VAT composite plates can not be determined by the thermal strains. Ignoring this fact would result in an incorrect prediction of pre-buckled load and thus have a certain effect on the evaluation of buckling load of VAT composite plates. A comparsion study has been examined on the distributions of in-plane force resultant obtained by the Rayleigh-Ritz method, FE method and Eq. 60 for the tow-steered plate $[\pm\langle 66.05|11.73\rangle]_s$ under Type-B boundary constraint. It was found that the results obtained by the present Rayleigh-Ritz method are very close to FE solutions, however, there exists a considerable discrepancy between the result given by Eq. 60 and FE solutions These results further demonstrate that the expressions given by Eq. 60 are not applicable for the evaluation of in-plane force resultant of variable stiffness composite panels under Type-B boundary constraint.

It is worth highlighting that for the straight-fibre format, if the symmetric-balanced layup is considered ($N_{xy}^{th} = 0$), the distributions of in-plane force resultant of the plate for both cases of Type-B and Type-C boundary constraints are identical [57]. In this regard, Eq. 60 can also be applied to predict the in-plane force resultants of symmetric-balanced straight-fibre plates subjected to Type-C boundary constraint, namely, all four edges are fixed against the in-plane normal displacements but are free to move tangentially. However, for symmetric-balanced VAT layups, there exists a considerable difference between the distributions of in-plane force resultant obtained under Type-B and Type-C boundary constraints. For the case of Type-C boundary constraint, the longitudinal force resultant N_x^0 of the plate is found to be constant over the entire plane, and meanwhile the in-plane shear force resultant N_{xy}^0 are zero everywhere, as described before. However, from Fig. 4, it can be clearly seen that both the longitudinal force resultant N_x^0 and in-plane shear force resultant N_{xy}^0 obtained under Type-B boundary constraint exhibit a highly nonuniform distribution over the entire plane, which are quite different from those obtained

Table 1: Critical buckling temperature ΔT_{cr} for both simply supported and clamped isotropic plates (unit: °C)

Boundary conditions	ΔT_{cr} (°C)					
	Present	Gossard [12]	Shariyat [25]	Prabhu [69]	Singha [70]	Nath [71]
Simply supported	63.23	63.27	62.14	63.21	63.266	63. 3
Clamped	167.26	168.71	166.91	169.07	167.856	168.0

Table 2: Critical buckling temperature ΔT_{cr} for single-layer square orthotropic plates with $\phi = 0°$ under clamped boundary condition (unit: °C)

Fibre orientation angle	ΔT_{cr} (°C)			
	Present	Shariyat [25]	Nath [71]	Huang [72]
$T_0 = T_1 = 0°$	151.59	151.6	153.0	152.47
$T_0 = T_1 = 45°$	131.77	130.43	133.3	131.88

under Type-C boundary constraint. These results again demonstrate that the in-plane boundary constraint has a significant influence on the in-plane thermoelastic behaviour of the tow-steered plate. Furthermore, by comparing the results obtained under Type-C and Type-D boundary constraints (Fig. 5 vs Fig. 6), it is clear that the distribution of in-plane force resultant is also greatly altered by the existing of uniform mechanical compression. Similar conclusions can be also drawn from Figs. 7 and 8, in which the distributions of in-plane force resultant are obtained under Type-E and Type-F boundary constraints, respectively.

Next, a model validation is performed on the thermal buckling analysis of isotropic plates ($a/h = 100$, $a/b = 1$, $\mu = 0.3$ and $\alpha = 2.0 \times 10^{-6}$/°C), which was initially studied by Gossard et al. [12]. As shown in Table. 1, the critical buckling temperatures predicted using the present Rayleigh-Ritz model for both simply supported and clamped isotropic plates correlate well with results previously published by Gossard et al [12], Prabhu and Dhanaraj [69], Singha et al [70], Nath and Shukla[71] and Shariyat [25].

A second verification of thermal buckling analysis is concentrated on a single-layer square orthotropic plate ($a/h = 40$ and $a/b = 1$) with clamped boundary conditions. Note, all four edges are fixed against in-plane normal and tangential displacements (Type-B boundary constraint). The Young's moduli, shear moduli, Possion's ratio and coefficients of thermal expansion for this composite material can be found in Ref. [72], in which critical buckling temperatures for plates have been calculated using both the Fourier series method (FSM) and the finite element method (FEM). The critical buckling temperatures obtained using the present Rayleigh-Ritz model are compared with the existing ones in Table. 2, and an excellent agreement between these results is reached, even for angle-ply layup configuration, which exhibits a considerable bending-twisting coupling.

To further validate the results, a model validation study on thermal buckling analysis is then extended to VAT composite plates. The layup configuration and geometric dimension of the plate are the same as those from the prebuckling model validation. However, several composite materials shown in Table. 3 are taken into account, which have been used for the thermal buckling optimization of VAT composite plates [50, 51]. In addition, the simply supported tow-steered plate is exposed to uniform temperature change and all four edges are fixed against the in-plane normal displacements but are free to move tangentially, that is, Type-C boundary constraint. The results of critical buckling temperature obtained by the present Rayleigh-Ritz method for VAT composite plates made of different composite materials are listed in Table. 4. The results published by Duran et al. [50], Vescovini and Dozio [48] and Zhao et al. [54] and FE solutions are also included for comparison purposes. It is noted that all VAT layup configurations listed in Table. 4 are the optimal results achieved by maximizing the thermal buckling load according to the optimization search [50]. From Table. 4, it is clear that the results of critical buckling temperature predicted by using the present Rayleigh-Ritz model are very close to those obtained by Vescovini and Dozio [48] and Zhao et al. [54] and FE solutions for all the composite materials studied. The ability of the proposed Rayleigh-Ritz model to accurately predict the thermal buckling response of VAT composite plates is thus demonstrated. However, for either Kevlar/Epoxy or Carbon/Epoxy materials, there is a big discrepancy in critical buckling temperature among results in Ref. [50] and obtained by other methods. The primary reason is that in Ref. [50], the distribution of pre-buckled load of VAT composite plates are predicted by directly using the thermal force resultants given by Eq. 60. These results further indicate that Eq. 60 is not applicable for accurately predicting the in-plane thermoelastic behaviour of symmetric-balanced tow-steered plates with Type C boundary constraint. A further investigation shows that for either Kevlar/Epoxy or Carbon/Epoxy materials, the difference in the buckling temperature between the results obtained using Eq. 60 and the present Rayleigh-Ritz results gradually decreases when the thermal expansion coefficient α_1 is changed from negative to positive. Similar phenomena

Table 3: Material and thermal properties of different composites

Material	E_{11}(Gpa)	E_{22}(Gpa)	G_{12}(Gpa)	v_{12}	$\alpha_{11}(\times 10^{-6}/°C)$	$\alpha_{22}(\times 10^{-6}/°C)$
Graphite/Epoxy	155	8.07	4.55	0.22	-0.07	30.1
E-Glass/Epoxy	41	10.04	4.3	0.28	7.0	26
S-Glass/Epoxy	45	11.0	4.5	0.29	7.1	30
Kevlar/Epoxy	80	5.5	2.2	0.34	-2.0	60
Carbon/Epoxy	147	10.3	7.0	0.27	-0.9	27
Carbon/Peek	138	8.7	5.0	0.28	-0.2	24
Carbon/Polyimide	216	5.0	4.5	0.25	0.0	25
Boron/Epoxy	201	21.7	5.4	0.17	6.1	30

can also be found in Ref. [73], in which a comparsion study of the thermal buckling temperature between the results predicted by the proposed finite element method combined with Eq. 60 and those computed using NASTRAN is conducted. Therefore, it can be conducted that the negative thermal expansion coefficient α_1 is responsible for this discrepancy, and in particular the greater the absolute value of thermal expansion coefficient α_1, the larger the discrepancy.

It is also noted that the numerical convergence of both prebuckling and buckling solutions of tow-steered plates with respect to the number of Legendre polynomial terms used in the Rayleigh-Ritz formulation has been examined in details. It was found that nine terms of displacement shape-function terms ($\underline{M+1, N+1}$; $\underline{R+1, S+1}$; $\underline{G+1, H+1}$) in the expressions of Eq. 55 or Eq. 56 are sufficient to yield accurate evaluation of buckling response of tow-steered plates as shown in Table. 4. On the other hand, in order to obtain the convergent results in prebuckling analysis, nine terms of Legendre polynomial ($\underline{P+1, Q+1}$) are required in the expansion form of Airy's stress function ϕ.

4.2. Thermal buckling response of VAT plates

This section mainly focuses on the influence of fibre orientation angle and boundary condition on the thermal buckling response of the tow-steered plate. The particular laminates exposed to uniform temperature change are square, approximately 25.4mm by 25.4 mm, and made of four 0.127mm-thick plies of graphite-epoxy prepreg, resulting in a total thickness $h = 0.508$mm. The layup configuration is denoted as $[\phi \pm \langle T_0 | T_1 \rangle]_s$, similar to that used in previous sections. The lamina properties are given by $E_{11} = 171$GPa, $E_{22} = 8.756$GPa, $G_{12} = G_{23} = G_{13} = 7.1$GPa and $v_{12} = v_{13} = v_{23} = 0.335$, which

Table 4: Critical buckling temperature ΔT_{cr} for VAT composite plates made of different composites (unit: °C)

Materials	$\langle T_0 \vert T_1 \rangle$	Present $M(N) \times P(Q) \times R(S)$					FEM	Vescovini [48]	Zhao [54]	Duran [50]
		$4 \times 4 \times 4$	$6 \times 6 \times 6$	$8 \times 8 \times 8$	$10 \times 10 \times 10$	$12 \times 12 \times 12$				
Graphite/Epoxy	$\langle 60.70 \vert 32.19 \rangle$	34.3634	33.4503	33.2280	33.1186	33.0607	33.084	33.0033	31.99	34.26
E-Glass/Epoxy	$\langle 6.710 \vert 58.04 \rangle$	5.5860	5.5625	5.5546	5.5519	5.5507	5.556	5.5546	5.48	5.58
S-Glass/Epoxy	$\langle 16.12 \vert 54.74 \rangle$	5.0604	5.0414	5.0358	5.0333	5.0321	5.037	5.0355	4.96	5.04
Kevlar/Epoxy	$\langle 66.05 \vert 11.73 \rangle$	17.3440	16.6074	16.5256	16.4915	16.4749	16.544	16.2708	16.09	$\boxed{22.18}$
Carbon/Epoxy	$\langle 69.00 \vert -5.705 \rangle$	38.5031	35.0856	34.7786	34.6607	34.5983	34.715	33.6616	33.80	$\boxed{57.79}$
Carbon/Peek	$\langle 63.07 \vert 29.50 \rangle$	37.3379	36.3547	36.1276	36.0186	35.9628	35.989	35.8670	34.93	38.08
Carbon/Polyimide	$\langle 56.30 \vert 36.68 \rangle$	81.2362	78.8101	78.1723	77.8440	77.6580	77.640	77.6006	74.89	78.28
Boron/Epoxy	$\langle -6.57 \vert 63.28 \rangle$	7.7118	7.6108	7.5677	7.5555	7.5487	7.554	7.5541	7.35	7.50

has been used for predicting thermally-induced deformation behaviours of unsymmetric laminates [22]. The thermal expansion coefficients are chosen to be $\alpha_1 = 0.283 \times 10^{-6}/°\mathrm{C}$ and $\alpha_2 = 15.34 \times 10^{-6}/°\mathrm{C}$ such that the plate will expand when heating or contract when cooling. Both simply supported (SSSS) and clamped (CCCC) boundary conditions are considered. Moreover, all four edges are fixed against the in-plane normal displacements but are free to move tangentially, that is, Type-C boundary constraint. The angle of rotation of the fibre path, due to the symmetry of boundary condition, is only chosen to be $\phi = 0°$, and meanwhile both fibre orientation angles T_0 and T_1 increase from 0° to 90° with a step of 15°. For the convenience of using as the benchmark for FEM and other numerical results, the results of critical buckling temperature of tow-steered plates with various layup configurations obtained using the present Rayleigh-Ritz model are presented in Tables. 5 and 6 for SSSS and CCCC boundary conditions, respectively.

From Tables. 5 and6, it is clear that for each case, the critical buckling temperature of the tow-steered plate varies with both fibre orientation angles T_0 and T_1, which provides more additional freedom in stiffness tailoring to achieve better thermal buckling resistance when compared to those with straight-fibre formats. In particular, for the case of CCCC boundary condition, the maximum buckling temperature of the plate subjected to Type-C boundary constraint is achieved by the VAT layup configuration $[\pm\langle 60 \vert 0 \rangle]_s$, in which a 15.66% increase in thermal buckling resistance is observed when compared to the maximum value given by the straight-fibre format. These results highlight the distinct superiority of using the tow-steered technology to enhance the thermal buckling response of composite laminates. Furthermore, it is found that the critical buckling temperature ob-

Table 5: Critical buckling temperature ΔT_{cr} for simply supported tow-steered plates under Type-C boundary constraint (unit: °C)

T_0 \ T_1	0	15	30	45	60	75	90
0	230.2	256.2	319.9	372.5	366.8	319.4	253.8
15	251.2	298.6	352.3	376.4	365.3	313.1	249.1
30	302.1	325.4	361.8	383.0	365.9	310.5	250.9
45	304.6	334.1	371.1	387.6	366.0	311.9	260.5
60	304.5	337.0	371.5	383.2	361.8	317.4	278.1
75	297.9	328.9	356.5	361.9	344.5	298.6	247.9
90	296.9	322.9	340.2	336.8	304.4	256.1	230.2

tained under CCCC boundary condition is always higher than that obtained under SSSS boundary condition, which means that the thermal buckling resistance can be improved to a certain degree by strengthening out-of-plane boundary constraints. In addition, it is interesting to note that if the symmetric-balanced layup configuration is considered, the results of critical buckling temperature of the straight-fibre plate obtained under either the Type-B or Type-C boundary constraint are the same as each other. However, this may be not the case for VAT layup configurations. A further in-depth study on tow-steered plates shows that even though there exists a considerable difference between the distributions of in-plane force resultant obtained under Type-B and Type-C boundary constraints, the maximum difference between the critical buckling temperatures obtained under Type-B and Type-C boundary constraints is kept within 2%, which indicates the in-plane shear constraint along the boundary edges of the plate has only a slight influence on the evaluation of critical buckling temperature of symmetric-balanced tow-steered plates.

4.3. Thermomechanical buckling response of VAT plates

In this section, the thermomechanical buckling response of VAT composite plates is investigated with emphasis on considering the influence of the temperature change on the compressive performance of the tow-steered plate. The mechanism of applying tow-steered technology to improve the thermomechanical buckling resistance of composite plates is also explored. The geometric dimension, material property and layup configuration of the plate are the same as those in Section. 4.2. Herein, the plate is simply

Table 6: Critical buckling temperature ΔT_{cr} for clamped tow-steered plates under Type-C boundary constraint (unit: °C)

T_0 \ T_1	0	15	30	45	60	75	90
0	521.2	531.0	546.1	571.3	589.4	546.7	524.7
15	559.9	589.4	629.3	675.5	622.7	575.5	554.8
30	679.4	739.8	787.2	733.3	670.2	625.7	609.1
45	880.3	877.9	840.4	787.1	734.4	697.2	669.0
60	910.5	901.6	871.3	831.4	787.2	686.6	623.3
75	905.9	885.2	845.2	748.3	654.3	589.4	557.9
90	823.3	754.4	684.2	620.1	568.6	536.3	521.2

supported on four edges and subjected to Type-D boundary constraint. A preliminary study was conducted on the thermal buckling analysis for the tow-steered plate under Type-C boundary constraint. It was found that the lowest bucking temperature is obtained by the straight-fibre format $[\pm 90]_s$, that is, $\Delta T_{cr} = 230.2$°C. In view of this, a 200°C temperature difference between the stress-free and operational temperatures will be imposed on the plate such that the tow-steered plate with each layup configuration still remains unbuckled before uniform mechanical compression is applied. As such, three cases of temperature change, that is, $\Delta T = -200$°C, $\Delta T = 0$°C and $\Delta T = 200$°C, are taken into account. $\Delta T = -200$°C and $\Delta T = 200$°C denotes the cooling and heating process on the plate, respectively, while $\Delta T = 0$°C represents the stress-free temperature state, in which the buckling of the plate is only governed by uniform mechanical compression. Two types of laminates are used for study, that is, $\phi = 0°$ and $\phi = 90°$, such that the fibre angle and thus the stiffness within the plate are only a function of the x or the y coordinate, respectively. For the former case, the longitudinal force resultant N_x^0 is constant everywhere, whereas for the latter case, the longitudinal force resultant N_x^0 is only a function of the y coordinate. Note that, the average critical buckling load N_{xcr}^{av} is evaluated by the following expression [49]:

$$N_{xcr}^{av} = \lambda^{(1)} N_{xcr}^{av(1)} + \lambda^{(2)} N_{xcr}^{av(2)} \tag{61}$$

where $N_{xcr}^{av(1)}$ and $N_{xcr}^{av(2)}$ are the average longitudinal load along $x = \pm a/2$ obtained under pure thermal and mechanical loadings, respectively. For comparison purposes, the buckling coefficient K_{cr} is introduced to normalize the the average critical buckling load N_{xcr}^{av} [1], that is,

$$K_{\mathrm{cr}} = N_{xcr}^{av} a^2 / E_{11} h^3 \tag{62}$$

Normalized critical buckling loads of the tow-steered plate with various layup configurations obtained using the present Rayleigh-Ritz model are shown in Fig. 9-11 for different combinations of plate-type and temperature change. Note that, each curve in the figures represents a series of VAT panels generated by varying T_1 from 0° at the left-end to 90° at the right-end, but with a same value of T_0, which is labelled in each figure. From Fig. 9-11 and Figs. 13-15, it is clear that for each combination of plate type and temperature change, the critical buckling load of the plate varies with both fibre orientation angles T_0 and T_1, which further indicates that the VAT layup configurations always exhibit an extended freedom in stiffness tailoring to achieve better buckling performance.

For the case of $\phi = 0°$, if no temperature change is taken into account, that is, $\Delta T = 0$°C, the maximum value of buckling coefficient K_{cr} is 1.17, and is achieved by the VAT layup configuration of $T_0 = 0°$ and $T_1 = 45°$, which is 16.21% higher than the maximum value offered by the straight-fibre format $[\pm 0]_s$. This slight increase in buckling coefficient over straight-fibre plates is primarily attributed to the favorable distribution of transverse force resultant N_y^0 over the plate domain, as explained by Gürdal et al. [1]. Similar conclusion can also be observed from Figs. 9 and 11, in which VAT composite plates are respectively subjected to cooling and heating loadings in addition to uniform compression loadings. These findings indicate that the mechanism behind a slight improvement of buckling performance almost remains in effect in the thermomechanical buckling regime. For example, when the temperature change is $\Delta T = 200$°C, the tow-steered plate $[\pm\langle 0|45\rangle]_s$ exhibits higher buckling performance compared to other linear fibre variations, and in particular, a 16.47% increase in buckling coefficient is observed when compared to the maximum value of the straight-fibre format $[\pm 30]_s$.

By comparing the results presented in Figs. 9-11, it can be found that the buckling performance of the tow-steered plate is also greatly affected by the temperature change. For most VAT layup configurations, the buckling coefficient of the plate increases when the temperature falls below the reference temperature, and decreases when the temperature rises above the reference temperature. However, a further investigation reveals that the variation of buckling load with temperature difference is closely related to the difference of mechanical and thermal buckling coefficients, that is, $\Delta K_{cr} = K_{cr}^{(2)} - K_{cr}^{(1)}$. Note that, the mechanical and thermal buckling coefficients ($K_{cr}^{(2)}$ and $K_{cr}^{(1)}$) are obtained under pure mechanical and thermal loadings, respectively. For VAT layups with $\Delta K_{cr} > 0$, the buckling coefficient of the tow-steered plate increases when $\Delta T < 0$°C and decreases when $\Delta T > 0$°C, whereas for VAT layups with $\Delta K_{cr} < 0$, the tow-steered plate give a completely opposite result. For example, for both VAT layups $[\pm\langle 0|45\rangle]_s$ and $[\pm\langle 60|75\rangle]_s$, the difference between mechanical and thermal buckling coefficients is positive ($\Delta K_{cr} > 0$) and negative ($\Delta K_{cr} < 0$), respectively. For the former case, the plate at $\Delta T = -200$°C exhibits a 27.57% increase in the buckling load when compared to that at the reference temperature, whereas for the latter case, the plate at $\Delta T = -200$°C shows a lower buckling coefficient than that at $\Delta T = 0$°C, even though the residual thermal stresses reduce the combined resultant stress near the panel center. There results indicate that the buckling performance of the tow-steered plate under a combination of thermal and mechanical loadings is a result of the thermomechanical coupling interaction. The normalized buckling loads for both VAT layups $[\pm\langle 0|45\rangle]_s$ and $[\pm\langle 60|75\rangle]_s$ are plotted in Fig. 12 as a function of temperature difference ΔT.

For the combination of $\phi = 90°$ and $\Delta T = 0$°C, the VAT layup $[90 \pm \langle 0|90\rangle]_s$ has the highest buckling coefficient among all the VAT layup configurations $[\phi \pm \langle T_0|T_1\rangle]_s$ with linear variation of fibre angles, and in particular a 23.09% increase in the buckling load is found when compared to the maximum value given by the straight-fibre format $[\pm 0]_s$. However, this improvement is due to the redistribution of the longitudinal compression load away from the central region towards the simply supported edge, which is different from that in the case of $\phi = 0°$. Furthermore, it is clearly seen from Figs. 13 and 15 that for both combinations of $\phi = 90°, \Delta T = -200$°C and $\phi = 90°, \Delta T = 200$°C, the overall curves that represent normalized buckling loads of VAT composite plates are nearly the same as those in Fig. 14, which indicates that the load redistribution is still the main driver for the improvement in buckling resistance, even if there exists temperature change. For instance, for the case of $\Delta T = -200$°C, the VAT layup $[90 \pm \langle 0|90\rangle]_s$ still exhibits higher buckling performance when compared to other linear fibre variations, and a 31.69% increase in buckling coefficient is observed when compared to the maximum value offered by the straight-fibre format $[\pm 0]_s$. These results further demonstrate the distinct superiority of applying the variable angle tow concept to improve buckling resistance of composite plates under combinated thermal and mechanical loadings.

In addition, the temperature change also has a significant influence on the buckling behaviour of the tow-steered plate. It is found that even for the case of $\phi = 90°$, the variation of buckling load with temperature difference also has a close connection with the difference of the mechanical and thermal buckling coefficients, that is, $\Delta K_{cr} = K_{cr}^{(2)} - K_{cr}^{(1)}$. As described before, for VAT layups with $\Delta K_{cr} > 0$, a certain increase in buckling resistance is achieved by the tow-steered plate when $\Delta T < 0°$C , while a certain decrease in buckling resistance is obtained by the tow-steered plate when $\Delta T > 0°$C. For VAT layups with $\Delta K_{cr} < 0$, however, the tow-steered plate gives a completely opposite result. The thermomechanical coupling interaction is responsible for this variation of buckling load with temperature difference. In particular, for the VAT layup $[90 \pm \langle 0|90 \rangle]_s$, the buckling load obtained under pure compression loadings is higher than that obtained under pure thermal loadings, that is, $\Delta K_{cr} > 0$. Accordingly, the buckling load at $\Delta T = -200°$C exhibits 47.97% higher than that at the reference temperature. This result further explains the experimental phenomenon in tests of variable stiffness composite plates under residual thermal stress condition, which were observed by Wu et al. [10]. However, for some particular VAT layups such as $[90 \pm \langle 45|0 \rangle]_s$, the buckling load obtained under pure compression loadings is lower than that obtained under pure thermal loadings, that is, $\Delta K_{cr} < 0$. For this case, the plate at $\Delta T = -200°$C shows a lower buckling coefficient when compared to that at stress-free temperature state, even though the residual thermal stress resultant distribution reduce the combined resultant stress near the panel center. The normalized buckling loads for both VAT layups $[90 \pm \langle 0|90 \rangle]_s$ and $[90 \pm \langle 45|0 \rangle]_s$ are plotted in Fig. 16 as a function of temperature difference ΔT.

5. Conclusion

In this paper, methodologies based on the generalised Rayleigh-Ritz method were applied for the in-plane thermoelastic and thermomechanical buckling analysis of symmetrical VAT composite plates under a combination of temperature change and general boundary constraint. In the framework of thermoelastic theory, the in-plane thermoelastic problem was firstly solved to determine the non-uniform distribution of in-plane force resultant of the tow-steered plate and the governing equation of thermomechanical buckling problem was then derived based on the third-order shear deformation theory of Reddy's type. The proposed modelling methodology has two novel aspects: First, the principle of thermoelastic complementary energy combined with Airy's stress function formulation, for the first time, was applied to solve the in-plane thermoelastic problem of the tow-steered plate; Second, the Lagrangian multiplier method was applied to release the restrictions inherent in the conventional Rayleigh-Ritz formulation, which provides generality to deal with general in-plane boundary constraint against thermal expansion or contraction. Numerical results on VAT plates under various in-plane boundary conditions demonstrated the accuracy and robustness of the proposed Rayleigh-Ritz model. Effects of the boundary constraint, fibre orientation angle, temperature difference on both in-plane thermoelastic and thermomechanical buckling performances of VAT composite plates were examined through various numerical case studies. Results have shown that both the in-plane thermoelastic and thermomechanical buckling behaviours of the tow-steered plate is strongly dependent on the in-plane boundary constraint and fibre orientation angle. Furthermore, the benign load redistribution mechanism offered by the VAT layup configuration was found to remain in effect even if there exists the temperature change. Also, it was found that the variation of buckling load with temperature difference is closely related to the difference of the mechanical and thermal buckling loads.

Acknowledgments

Xiaodong Chen would like to thank the financial support from the Special Fund for Doctoral Talents (Henan University of Urban Construction, China). Guojun Nie wish to acknowledge the financial support under the research project from National Natural Science Foundation of China (No. 11772232, 11372225 and 11072177). Zhangming Wu wish to acknowledge the financial support under A3 Talent Research Programme from Ningbo University, China.

Appendix

The elements of the matrices in Eq. (58) are expressed as following:

$$
\begin{aligned}
&K_{11}(mn,\overline{mn}) = \\
&\int_{-1}^{1}\int_{-1}^{1} c_1^2\left\{\left(\frac{4b}{a^3}H_{11}X^{w^0}_{\overline{m},\xi\xi}Y^{w^0}_{\overline{n}}+\frac{4}{ab}H_{12}X^{w^0}_{\overline{m}}Y^{w^0}_{\overline{n},\eta\eta}+\frac{8}{a^2}H_{16}X^{w^0}_{\overline{m},\xi}Y^{w^0}_{\overline{n},\eta}\right)X^{w^0}_{m,\xi\xi}Y^{w^0}_{n}+\right.\\
&\left(\frac{4}{ab}H_{12}X^{w^0}_{\overline{m},\xi\xi}Y^{w^0}_{\overline{n}}+\frac{4}{ab^3}H_{22}X^{w^0}_{\overline{m}}Y^{w^0}_{\overline{n},\eta\eta}+\frac{8}{b^2}H_{26}X^{w^0}_{\overline{m},\xi}Y^{w^0}_{\overline{n},\eta}\right)X^{w^0}_{m}Y^{w^0}_{n,\eta\eta}+\\
&\left.\left(\frac{8}{a^2}H_{16}X^{w^0}_{\overline{m},\xi\xi}Y^{w^0}_{\overline{n}}+\frac{8}{b^2}H_{26}X^{w^0}_{\overline{m}}Y^{w^0}_{\overline{n},\eta\eta}+\frac{16}{ab}H_{66}X^{w^0}_{\overline{m},\xi}Y^{w^0}_{\overline{n},\eta}\right)X^{w^0}_{m,\xi}Y^{w^0}_{n,\eta}\right\}\mathrm{d}\xi\mathrm{d}\eta+\\
&\int_{-1}^{1}\int_{-1}^{1}\left\{\left(\frac{a}{b}A_{44}X^{w^0}_{\overline{m}}Y^{w^0}_{\overline{n},\eta}+A_{45}X^{w^0}_{\overline{m},\xi}Y^{w^0}_{\overline{n}}-\frac{ac_2}{b}D_{44}X^{w^0}_{\overline{m}}Y^{w^0}_{\overline{n},\eta}-c_2D_{45}X^{w^0}_{\overline{m},\xi}Y^{w^0}_{\overline{n}}\right)X^{w^0}_{m}Y^{w^0}_{n,\eta}+\right.\\
&\left(A_{45}X^{w^0}_{\overline{m}}Y^{w^0}_{\overline{n},\eta}+\frac{b}{a}A_{55}X^{w^0}_{\overline{m},\xi}Y^{w^0}_{\overline{n}}-c_2D_{45}X^{w^0}_{\overline{m}}Y^{w^0}_{\overline{n},\eta}-\frac{bc_2}{a}D_{55}X^{w^0}_{\overline{m},\xi}Y^{w^0}_{\overline{n}}\right)X^{w^0}_{m,\xi}Y^{w^0}_{n}-\\
&c_2\left(\frac{a}{b}D_{44}X^{w^0}_{\overline{m}}Y^{w^0}_{\overline{n},\eta}+D_{45}X^{w^0}_{\overline{m},\xi}Y^{w^0}_{\overline{n}}-\frac{ac_2}{b}F_{44}X^{w^0}_{\overline{m}}Y^{w^0}_{\overline{n},\eta}-c_2F_{45}X^{w^0}_{\overline{m},\xi}Y^{w^0}_{\overline{n}}\right)X^{w^0}_{m}Y^{w^0}_{n,\eta}-\\
&\left.c_2\left(D_{45}X^{w^0}_{\overline{m}}Y^{w^0}_{\overline{n},\eta}+\frac{b}{a}D_{55}X^{w^0}_{\overline{m},\xi}Y^{w^0}_{\overline{n}}-c_2F_{45}X^{w^0}_{\overline{m}}Y^{w^0}_{\overline{n},\eta}-\frac{bc_2}{a}F_{55}X^{w^0}_{\overline{m},\xi}Y^{w^0}_{\overline{n}}\right)X^{w^0}_{m,\xi}Y^{w^0}_{n}\right\}\mathrm{d}\xi\mathrm{d}\eta
\end{aligned}
\tag{63}
$$

$$
\begin{aligned}
&K_{12}(mn,rs) = K_{21}(rs,mn) = \\
&\int_{-1}^{1}\int_{-1}^{1}\left\{\left(-\frac{2bc_1}{a^2}F_{11}X^{\phi_x^0}_{r,\xi}Y^{\phi_x^0}_{s}-\frac{2c_1}{a}F_{16}X^{\phi_x^0}_{r}Y^{\phi_x^0}_{s,\eta}+\frac{2bc_1^2}{a^2}H_{11}X^{\phi_x^0}_{r,\xi}Y^{\phi_x^0}_{s}+\frac{2c_1^2}{a}H_{16}X^{\phi_x^0}_{r}Y^{\phi_x^0}_{s,\eta}\right)X^{w^0}_{m,\xi\xi}Y^{w^0}_{n}+\right.\\
&\left(-\frac{2c_1}{b}F_{12}X^{\phi_x^0}_{r,\xi}Y^{\phi_x^0}_{s}-\frac{2ac_1}{b^2}F_{26}X^{\phi_x^0}_{r}Y^{\phi_x^0}_{s,\eta}+\frac{2c_1^2}{b}H_{12}X^{\phi_x^0}_{r,\xi}Y^{\phi_x^0}_{s}+\frac{2ac_1^2}{b^2}H_{26}X^{\phi_x^0}_{r}Y^{\phi_x^0}_{s,\eta}\right)X^{w^0}_{m}Y^{w^0}_{n,\eta\eta}+\\
&\left.\left(-\frac{4c_1}{a}F_{16}X^{\phi_x^0}_{r,\xi}Y^{\phi_x^0}_{s}-\frac{4c_1}{b}F_{66}X^{\phi_x^0}_{r}Y^{\phi_x^0}_{s,\eta}+\frac{4c_1^2}{a}H_{16}X^{\phi_x^0}_{r,\xi}Y^{\phi_x^0}_{s}+\frac{4c_1^2}{b}H_{66}X^{\phi_x^0}_{r}Y^{\phi_x^0}_{s,\eta}\right)X^{w^0}_{m,\xi}Y^{w^0}_{n,\eta}\right\}\mathrm{d}\xi\mathrm{d}\eta+\\
&\int_{-1}^{1}\int_{-1}^{1}\left\{\left(\frac{a}{2}A_{45}-ac_2D_{45}+\frac{ac_2^2}{2}F_{45}\right)X^{\phi_x^0}_{r}Y^{\phi_x^0}_{s}X^{w^0}_{m}Y^{w^0}_{n,\eta}+\right.\\
&\left.\left(\frac{b}{2}A_{55}-bc_2D_{55}+\frac{bc_2^2}{2}F_{55}\right)X^{\phi_x^0}_{r}Y^{\phi_x^0}_{s}X^{w^0}_{m,\xi}Y^{w^0}_{n}\right\}\mathrm{d}\xi\mathrm{d}\eta
\end{aligned}
\tag{64}
$$

$$
\begin{aligned}
&K_{13}(mn,gh) = K_{31}(gh,mn) = \\
&\int_{-1}^{1}\int_{-1}^{1}\left\{\left(-\frac{2c_1}{a}F_{12}X_g^{\phi_y^0}Y_{h,\eta}^{\phi_y^0} - \frac{2bc_1}{a^2}F_{16}X_{g,\xi}^{\phi_y^0}Y_h^{\phi_y^0} + \frac{2c_1^2}{a}H_{12}X_g^{\phi_y^0}Y_{h,\eta}^{\phi_y^0} + \frac{2bc_1^2}{a^2}H_{16}X_{g,\xi}^{\phi_y^0}Y_h^{\phi_y^0}\right)X_{m,\xi\xi}^{w^0}Y_n^{w^0} + \right. \\
&\left(-\frac{2ac_1}{b^2}F_{22}X_g^{\phi_y^0}Y_{h,\eta}^{\phi_y^0} - \frac{2c_1}{b}F_{26}X_{g,\xi}^{\phi_y^0}Y_h^{\phi_y^0} + \frac{2ac_1^2}{b^2}H_{22}X_g^{\phi_y^0}Y_{h,\eta}^{\phi_y^0} + \frac{2c_1^2}{b}H_{26}X_{g,\xi}^{\phi_y^0}Y_h^{\phi_y^0}\right)X_m^{w^0}Y_{n,\eta\eta}^{w^0} + \\
&\left.\left(-\frac{4c_1}{b}F_{26}X_g^{\phi_y^0}Y_{h,\eta}^{\phi_y^0} - \frac{4c_1}{a}F_{66}X_{g,\xi}^{\phi_y^0}Y_h^{\phi_y^0} + \frac{4c_1^2}{b}H_{26}X_g^{\phi_y^0}Y_{h,\eta}^{\phi_y^0} + \frac{4c_1^2}{a}H_{66}X_{g,\xi}^{\phi_y^0}Y_h^{\phi_y^0}\right)X_{m,\xi}^{w^0}Y_{n,\eta}^{w^0}\right\}\mathrm{d}\xi\mathrm{d}\eta + \\
&\int_{-1}^{1}\int_{-1}^{1}\left\{\left(\frac{a}{2}A_{44} - ac_2D_{44} + \frac{ac_2^2}{2}F_{44}\right)X_g^{\phi_y^0}Y_h^{\phi_y^0}X_m^{w^0}Y_{n,\eta}^{w^0} + \right. \\
&\left.\left(\frac{b}{2}A_{45} - bc_2D_{45} + \frac{bc_2^2}{2}F_{45}\right)X_g^{\phi_y^0}Y_h^{\phi_y^0}X_{m,\xi}^{w^0}Y_n^{w^0}\right\}\mathrm{d}\xi\mathrm{d}\eta
\end{aligned}
\tag{65}
$$

$$
\begin{aligned}
&K_{22}(rs,\overline{rs}) = \\
&\int_{-1}^{1}\int_{-1}^{1}\left\{\left(\frac{b}{a}D_{11}X_{\bar{r},\xi}^{\phi_x^0}Y_{\bar{s}}^{\phi_x^0} + D_{16}X_{\bar{r}}^{\phi_x^0}Y_{\bar{s},\eta}^{\phi_x^0} - \frac{bc_1}{a}F_{11}X_{\bar{r},\xi}^{\phi_x^0}Y_{\bar{s}}^{\phi_x^0} - c_1F_{16}X_{\bar{r}}^{\phi_x^0}Y_{\bar{s},\eta}^{\phi_x^0}\right)X_{r,\xi}^{\phi_x^0}Y_s^{\phi_x^0} + \right. \\
&\left(D_{16}X_{\bar{r},\xi}^{\phi_x^0}Y_{\bar{s}}^{\phi_x^0} + \frac{a}{b}D_{66}X_{\bar{r}}^{\phi_x^0}Y_{\bar{s},\eta}^{\phi_x^0} - c_1F_{16}X_{\bar{r},\xi}^{\phi_x^0}Y_{\bar{s}}^{\phi_x^0} - \frac{ac_1}{b}F_{66}X_{\bar{r}}^{\phi_x^0}Y_{\bar{s},\eta}^{\phi_x^0}\right)X_r^{\phi_x^0}Y_{s,\eta}^{\phi_x^0} + \\
&\left(-\frac{bc_1}{a}F_{11}X_{\bar{r},\xi}^{\phi_x^0}Y_{\bar{s}}^{\phi_x^0} - c_1F_{16}X_{\bar{r}}^{\phi_x^0}Y_{\bar{s},\eta}^{\phi_x^0} + \frac{bc_1^2}{a}H_{11}X_{\bar{r},\xi}^{\phi_x^0}Y_{\bar{s}}^{\phi_x^0} + c_1^2H_{16}X_{\bar{r}}^{\phi_x^0}Y_{\bar{s},\eta}^{\phi_x^0}\right)X_{r,\xi}^{\phi_x^0}Y_s^{\phi_x^0} + \\
&\left.\left(-c_1F_{16}X_{\bar{r},\xi}^{\phi_x^0}Y_{\bar{s}}^{\phi_x^0} - \frac{ac_1}{b}F_{66}X_{\bar{r}}^{\phi_x^0}Y_{\bar{s},\eta}^{\phi_x^0} + c_1^2H_{16}X_{\bar{r},\xi}^{\phi_x^0}Y_{\bar{s}}^{\phi_x^0} + \frac{ac_1^2}{b}H_{66}X_{\bar{r}}^{\phi_x^0}Y_{\bar{s},\eta}^{\phi_x^0}\right)X_r^{\phi_x^0}Y_{s,\eta}^{\phi_x^0}\right\}\mathrm{d}\xi\mathrm{d}\eta + \\
&\int_{-1}^{1}\int_{-1}^{1}\left(\frac{ab}{4}A_{55} - \frac{abc_2}{2}D_{55} + \frac{abc_2^2}{4}F_{55}\right)X_{\bar{r}}^{\phi_x^0}Y_{\bar{s}}^{\phi_x^0}X_r^{\phi_x^0}Y_s^{\phi_x^0}\mathrm{d}\xi\mathrm{d}\eta
\end{aligned}
\tag{66}
$$

$$K_{23}(rs,gh) = K_{32}(gh,rs) =$$

$$\int_{-1}^{1}\int_{-1}^{1}\left\{\left(D_{12}X_{g}^{\phi_y^0}Y_{h,\eta}^{\phi_y^0} + \frac{b}{a}D_{16}X_{g,\xi}^{\phi_y^0}Y_{h}^{\phi_y^0} - c_1F_{12}X_{g}^{\phi_y^0}Y_{h,\eta}^{\phi_y^0} - \frac{bc_1}{a}F_{16}X_{g,\xi}^{\phi_y^0}Y_{h}^{\phi_y^0}\right)X_{r,\xi}^{\phi_x^0}Y_{s}^{\phi_x^0} + \right.$$
$$\left(\frac{a}{b}D_{26}X_{g}^{\phi_y^0}Y_{h,\eta}^{\phi_y^0} + D_{66}X_{g,\xi}^{\phi_y^0}Y_{h}^{\phi_y^0} - \frac{ac_1}{b}F_{26}X_{g}^{\phi_y^0}Y_{h,\eta}^{\phi_y^0} - c_1F_{66}X_{g,\xi}^{\phi_y^0}Y_{h}^{\phi_y^0}\right)X_{r}^{\phi_x^0}Y_{s,\eta}^{\phi_x^0} +$$
$$\left(-c_1F_{12}X_{g}^{\phi_y^0}Y_{h,\eta}^{\phi_y^0} - \frac{bc_1}{a}F_{16}X_{g,\xi}^{\phi_y^0}Y_{h}^{\phi_y^0} + c_1^2H_{12}X_{g}^{\phi_y^0}Y_{h,\eta}^{\phi_y^0} + \frac{bc_1^2}{a}H_{16}X_{g,\xi}^{\phi_y^0}Y_{h}^{\phi_y^0}\right)X_{r,\xi}^{\phi_x^0}Y_{s}^{\phi_x^0} +$$
$$\left.\left(-\frac{ac_1}{b}F_{26}X_{g}^{\phi_y^0}Y_{h,\eta}^{\phi_y^0} - c_1F_{66}X_{g,\xi}^{\phi_y^0}Y_{h}^{\phi_y^0} + \frac{ac_1^2}{b}H_{26}X_{g}^{\phi_y^0}Y_{h,\eta}^{\phi_y^0} + c_1^2H_{66}X_{g,\xi}^{\phi_y^0}Y_{h}^{\phi_y^0}\right)X_{r}^{\phi_x^0}Y_{s,\eta}^{\phi_x^0}\right\}\mathrm{d}\xi\mathrm{d}\eta +$$
$$\int_{-1}^{1}\int_{-1}^{1}\left(\frac{ab}{4}A_{45} - \frac{abc_2}{2}D_{45} + \frac{abc_2^2}{4}F_{45}\right)X_{g}^{\phi_y^0}Y_{h}^{\phi_y^0}X_{r}^{\phi_x^0}Y_{s}^{\phi_x^0}\mathrm{d}\xi\mathrm{d}\eta \tag{67}$$

$$K_{33}(gh,\overline{g}\overline{h}) =$$

$$\int_{-1}^{1}\int_{-1}^{1}\left\{\left(\frac{a}{b}D_{22}X_{\overline{g}}^{\phi_y^0}Y_{\overline{h},\eta}^{\phi_y^0} + D_{26}X_{\overline{g},\xi}^{\phi_y^0}Y_{\overline{h}}^{\phi_y^0} - \frac{ac_1}{b}F_{22}X_{\overline{g}}^{\phi_y^0}Y_{\overline{h},\eta}^{\phi_y^0} - c_1F_{26}X_{\overline{g},\xi}^{\phi_y^0}Y_{\overline{h}}^{\phi_y^0}\right)X_{g}^{\phi_y^0}Y_{h,\eta}^{\phi_y^0} + \right.$$
$$\left(D_{26}X_{\overline{g}}^{\phi_y^0}Y_{\overline{h},\eta}^{\phi_y^0} + \frac{b}{a}D_{66}X_{\overline{g},\xi}^{\phi_y^0}Y_{\overline{h}}^{\phi_y^0} - c_1F_{26}X_{\overline{g}}^{\phi_y^0}Y_{\overline{h},\eta}^{\phi_y^0} - \frac{bc_1}{a}F_{66}X_{\overline{g},\xi}^{\phi_y^0}Y_{\overline{h}}^{\phi_y^0}\right)X_{g,\xi}^{\phi_y^0}Y_{h}^{\phi_y^0} +$$
$$\left(-\frac{ac_1}{b}F_{22}X_{\overline{g}}^{\phi_y^0}Y_{\overline{h},\eta}^{\phi_y^0} - c_1F_{26}X_{\overline{g},\xi}^{\phi_y^0}Y_{\overline{h}}^{\phi_y^0} + \frac{ac_1^2}{b}H_{22}X_{\overline{g}}^{\phi_y^0}Y_{\overline{h},\eta}^{\phi_y^0} + c_1^2H_{26}X_{\overline{g},\xi}^{\phi_y^0}Y_{\overline{h}}^{\phi_y^0}\right)X_{g}^{\phi_y^0}Y_{h,\eta}^{\phi_y^0} +$$
$$\left.\left(-c_1F_{26}X_{\overline{g}}^{\phi_y^0}Y_{\overline{h},\eta}^{\phi_y^0} - \frac{bc_1}{a}F_{66}X_{\overline{g},\xi}^{\phi_y^0}Y_{\overline{h}}^{\phi_y^0} + c_1^2H_{26}X_{\overline{g}}^{\phi_y^0}Y_{\overline{h},\eta}^{\phi_y^0} + \frac{bc_1^2}{a}H_{66}X_{\overline{g},\xi}^{\phi_y^0}Y_{\overline{h}}^{\phi_y^0}\right)X_{g,\xi}^{\phi_y^0}Y_{h}^{\phi_y^0}\right\}\mathrm{d}\xi\mathrm{d}\eta +$$
$$\int_{-1}^{1}\int_{-1}^{1}\left(\frac{ab}{4}A_{44} - \frac{abc_2}{2}D_{44} + \frac{abc_2^2}{4}F_{44}\right)X_{\overline{g}}^{\phi_y^0}Y_{\overline{h}}^{\phi_y^0}X_{g}^{\phi_y^0}Y_{h}^{\phi_y^0}\mathrm{d}\xi\mathrm{d}\eta \tag{68}$$

$$L_{11}(mn,\overline{mn}) =$$
$$\int_{-1}^{1}\int_{-1}^{1}\left\{\left(\frac{b}{a}N_x^0X_{\overline{m},\xi}^{w^0}Y_{\overline{n}}^{w^0} + N_{xy}^0X_{\overline{m}}^{w^0}Y_{\overline{n},\eta}^{w^0}\right)X_{m,\xi}^{w^0}Y_{n}^{w^0} + \right.$$
$$\left.\left(\frac{a}{b}N_y^0X_{\overline{m}}^{w^0}Y_{\overline{n},\eta}^{w^0} + N_{xy}^0X_{\overline{m},\xi}^{w^0}Y_{\overline{n}}^{w^0}\right)X_{m}^{w^0}Y_{n,\eta}^{w^0}\right\}\mathrm{d}\xi\mathrm{d}\eta \tag{69}$$

where $m,\overline{m} = 0,1,2\cdots,M$; $n,\overline{n} = 0,1,2\cdots,N$; $r,\overline{r} = 0,1,2\cdots,R$; $s,\overline{s} = 0,1,2\cdots,S$; $g,\overline{g} = 0,1,2\cdots,G$; $h,\overline{h} = 0,1,2\cdots,H$. The terms $X_m^{w^0}$, $Y_n^{w^0}$, $X_r^{\phi_x^0}$, $Y_s^{\phi_x^0}$, $X_g^{\phi_y^0}$, $Y_h^{\phi_y^0}$

are constructed by Legendre polynomials multiplying with the functions that satisfy the geometrical boundary condition at the edges of VAT composite plates. For instance, if the plate is clamped on four edges, the terms $X_m^{w^0}$, $Y_n^{w^0}$, $X_r^{\phi_x^0}$, $Y_s^{\phi_x^0}$, $X_g^{\phi_y^0}$, $Y_h^{\phi_y^0}$ can be written as:

$$
\begin{aligned}
&X_m^{w^0}(\xi) = (1-\xi^2)L_m(\xi); \quad Y_n^{w^0}(\eta) = (1-\eta^2)L_n(\eta) \\
&X_r^{\phi_x^0}(\xi) = (1-\xi^2)L_r(\xi); \quad Y_s^{\phi_x^0}(\eta) = (1-\eta^2)L_s(\eta) \\
&X_g^{\phi_y^0}(\xi) = (1-\xi^2)L_g(\xi); \quad Y_h^{\phi_y^0}(\eta) = (1-\eta^2)L_h(\eta)
\end{aligned}
\tag{70}
$$

If the plate is simply supported on four edges, the terms $X_m^{w^0}$, $Y_n^{w^0}$, $X_r^{\phi_x^0}$, $Y_s^{\phi_x^0}$, $X_g^{\phi_y^0}$, $Y_h^{\phi_y^0}$ can be written as:

$$
\begin{aligned}
&X_m^{w^0}(\xi) = (1-\xi^2)L_m(\xi); \quad Y_n^{w^0}(\eta) = (1-\eta^2)L_n(\eta) \\
&X_r^{\phi_x^0}(\xi) = L_r(\xi); \quad Y_s^{\phi_x^0}(\eta) = (1-\eta^2)L_s(\eta) \\
&X_g^{\phi_y^0}(\xi) = (1-\xi^2)L_g(\xi); \quad Y_h^{\phi_y^0}(\eta) = L_h(\eta)
\end{aligned}
\tag{71}
$$

References

[1] Z. Gürdal, B. Tatting, C. Wu, Variable stiffness composite panels: Effects of stiffness variation on the in-plane and buckling response, Composites Part A: Applied Science and Manufacturing 39 (2008) 911–922.

[2] S. T. IJsselmuiden, M. M. Abdalla, Z. Gürdal, Optimization of variable-stiffness panels for maximum buckling load using lamination parameters, AIAA Journal 48 (2010) 134–143.

[3] Z. Wu, P. M. Weaver, G. Raju, B. C. Kim, Buckling analysis and optimisation of variable angle tow composite plates, Thin Walled Structures 60 (2012) 163–172.

[4] G. Raju, Z. Wu, B. Kim, P. M. Weaver, Prebuckling and buckling analysis of variable angle tow plates with general boundary conditions, Composite Structures 94 (2012) 2961–2970.

[5] Z. Wu, G. Raju, P. M. Weaver, Framework for the buckling optimization of variable angle tow composite plates, AIAA Journal 53 (2015) 3788–3804.

[6] P. Hao, C. Liu, X. Yuan, B. Wang, G. Li, T. Zhu, F. Niu, Buckling optimization of variable-stiffness composite panels based on flow field function, Composite Structures 181 (2017) 240–255.

[7] X. Chen, Z. Wu, G. Nie, P. Weaver, Buckling analysis of variable angle tow composite plates with a through-the-width or an embedded rectangular delamination, International Journal of Solids and Structures 138 (2018) 166–180.

[8] Z. Wu, G. Raju, P. M. Weaver, Optimization of postbuckling behaviour of variable thickness composite panels with variable angle tows: Towards "buckle-free" design concept, International Journal of Solids and Structures 132-133 (2018) 66–79.

[9] X. Chen, G. Nie, Prebuckling and buckling analysis of moderately thick variable angle tow composite plates considering the extension-shear coupling, Composite Structures 242 (2020). Doi: 10.1016/j.compstruct.2020.112093.

[10] K. C. Wu, Z. Gürdal, J. H. Starnes, Structural response of compression-loaded, tow-placed, variable stiffness composite panels, in: 43th AIAA/ASME/ASCE/AHS/ASC Structures, Structural Dynamics and Materials Conference, AIAA 2002-1512, Denver, CO.

[11] H. W. Bargmann, Thermal buckling of elastic plates, Journal of Thermal Stresses 8 (1985) 71–98.

[12] M. L. Gossard, P. Seide, W. M. Roberts, Thermal Buckling of Plates,, Technical Note 2771, NACA, 1952.

[13] N. J. Hoff, Thermal buckling of supersonic wing panels, Journal of the Aeronautical Sciences 23 (1956) 1019–1028.

[14] N. J. Hoff, Buckling at high temperature, Journal of the Royal Aeronautical Society 61 (1957) 756–774.

[15] M. S. S. Prabhu, S. Durvasula, Elastic stability of thermally stressed clamped-clamped skew plates, Journal of Applied Mechanics 41 (1974) 820–821.

[16] L.-W. Chen, E. J. Brunelle, L. Y. Chen, Thermal buckling of initially stressed thick plates, Journal of Mechanical Design 104 (1982) 557–564.

[17] J. M. Whitney, J. E. Ashton, Effect of environment on the elastic response of layered composite plates, AIAA Journal 9 (1971) 1708–1713.

[18] T. R. Tauchert, N. N. Huang, Thermal Buckling of Symmetric Angle-ply Laminated Plates, Springer, Dordrecht, 1987.

[19] C. A. Meyers, M. W. Hyer, Thermal buckling and postbuckling of symmetrically laminated composite plates, Journal of Thermal Stresses 14 (1991) 519–540.

[20] L. X. Sun, T. R. Hsu, Thermal buckling of laminated composite plates with transverse shear deformation, Computers & Structures 36 (1990) 883–889.

[21] L. Librescu, M. A. Souza, Post-buckling of geometrically imperfect shear-deformable flat panels under combined thermal and compressive edge loadings, Journal of Applied Mechanics 60 (1993) 526–533.

[22] M. L. Dano, M. W. Hyer, Thermally-induced deformation behavior of unsymmetric laminates, International Journal of Solids & Structures 35 (1998) 2101–2120.

[23] H. S. Shen, Thermomechanical post-buckling analysis of imperfect laminated plates using a higher-order shear-deformation theory, Computers & Structures 66 (1998) 395–409.

[24] R. M. Jones, Thermal buckling of uniformly heated unidirectional and symmetric cross-ply laminated fiber-reinforced composite uniaxial in-plane restrained simply supported rectangular plates, Composites Part A: Applied Science and Manufacturing 36 (2005) 1355–1367.

[25] M. Shariyat, Thermal buckling analysis of rectangular composite plates with temperature-dependent properties based on a layerwise theory, Thin-Walled Structures 45 (2007) 439–452.

[26] X. Li, K. Yu, J. Han, H. Song, R. Zhao, Buckling and vibro-acoustic response of the clamped composite laminated plate in thermal environment, International Journal of Mechanical Sciences 119 (2016) 370–382.

[27] M. Cetkovic, Thermal buckling of laminated composite plates using layerwise displacement model, Composite Structures 142 (2016) 238–253.

[28] L. V. Tran, M. A. Wahab, S.-E. Kim, An isogeometric finite element approach for thermal bending and buckling analyses of laminated composite plates, Composite Structures 179 (2017) 35–49.

[29] J. Gutiérrez Álvarez, C. Bisagni, Closed-form solutions for thermomechanical buckling of orthotropic composite plates, Composite Structures 233 (2020). Doi: 10.1016/j.compstruct.2019.111622.

[30] L.-W. Chen, L.-Y. Chen, Thermal postbuckling behaviors of laminated composite plates with temperature-dependent properties, Composite Structures 19 (1991) 267–283.

[31] A. K. Noor, J. M. Peters, Thermomechanical buckling of multilayered composite plates, Journal of Engineering Mechanics 118 (1992) 351–366.

[32] G. Singh, G. V. Rao, N. G. R. Iyengar, Thermal postbuckling behavior of laminated composite plates, AIAA Journal 32 (1994) 1336–1338.

[33] Y. Shi, R. Y. Y. Lee, C. Mei, Thermal postbuckling of composite plates using the finite element modal coordinate method, Journal of Thermal Stresses 22 (1999) 595–614.

[34] J. S. Przemieniecki, Thermal stresses in rectangular plates, The Aeronautical Quarterly 10 (1959) 65–78.

[35] H. Parkus, Thermoelasticity, Springer-Verlag, New York, 2ed edition, 1976.

[36] M. W. Hyer, R. F. Charette, Use of curvilinear fiber format in composite structure design, AIAA Journal 29 (1991) 1011–1015.

[37] M. W. Hyer, H. H. Lee, The use of curvilinear fiber format to improve buckling resistance of composite plates with central circular holes, Composite Structures 18 (1991) 239–261.

[38] Z. Gürdal, R. Olmedo, In-plane response of laminates with spatially varying fiber orientations: variable stiffness concept, AIAA J 31 (1993) 751–758.

[39] R. Olmedo, Z. Gürdal, Buckling response of laminates with spatially varying fiber orientations, in: 34th AIAA/ASME/ASCE/AHS/ASC Structures, Structural Dynamics and Materials Conference, AIAA 93-1567, La Jolla, CA, pp. 2261–2269.

[40] Z. Wu, G. Raju, P. M. Weaver, Buckling of vat plates using energy methods, in: 53rd AIAA/ASME/ASCE/AHS/ASC Structures, Structural Dynamics and Materials Conference, AIAA 2012-1463, Honolulu, Hawaii.

[41] Z. Wu, G. Raju, P. M. Weaver, Postbuckling analysis of variable angle tow plates, International Journal of Solids and Structures 50 (2013) 1770–1780.

[42] G. Raju, Z. Wu, P. M. Weaver, Postbuckling analysis of variable angle tow plates using differential quadrature method, Composite Structures 106 (2013) 74–84.

[43] G. Zucco, R. M. J. Groh, A. Madeo, P. M. Weaver, Mixed shell element for static and buckling analysis of variable angle tow composite plates, Composite Structures 152 (2016) 324–338.

[44] B. H. Coburn, Z. Wu, P. M. Weaver, Buckling analysis of stiffened variable angle tow panels, Composite Structures 111 (2014) 259–270.

[45] V. Oliveri, A. Milazzo, A rayleigh-ritz approach for postbuckling analysis of variable angle tow composite stiffened panels, Computers & Structures (2017). Doi: 10.1016/j.compstruc.2017.10.009.

[46] R. Vescovini, V. Oliveri, D. Pizzi, L. Dozio, P. M. Weaver, A semi-analytical approach for the analysis of variable-stiffness panels with curvilinear stiffeners, International Journal of Solids and Structures 188-189 (2020) 244–260.

[47] A. Haldar, J. Reinoso, E. Jansen, R. Rolfes, Thermally induced multistable configurations of variable stiffness composite plates: Semi-analytical and finite element investigation, Composite Structures 183 (2018) 161–175.

[48] R. Vescovini, L. Dozio, Thermal buckling behaviour of thin and thick variable-stiffness panels, Journal of Composite Science 2 (2018). Doi: 10.3390/jcs2040058.

[49] M. M. Abdalla, Z. Gürdal, G. F. Abdelal, Thermomechanical response of variable stiffness composite panels, Journal of Thermal Stresses 32 (2008) 187–208.

[50] A. V. Duran, N. A. Fasanella, V. Sundararaghavan, A. M. Waas, Thermal buckling of composite plates with spatial varying fiber orientations, Composite Structures 124 (2015) 228–235.

[51] A. V. Duran, N. A. Fasanella, V. Sundararaghavan, A. M. Waas, Optimization of composite plates with spatially varying fiber paths for thermal buckling, in: 56th AIAA/ASCE/AHS/ASC Structures, Structural Dynamics and Materials Conference, AIAA 2015-0454, Kissimmee, Florida.

[52] M. Ganapathi, B. Anirudh, D. Aditya Narayan, C. Anant, B. Pradyumna, Thermal buckling behaviour of variable stiffness laminated composite plates, Materials Today Communications 16 (2018) 142–151.

[53] G. Zhang, J. Wang, A. Ni, S. Li, Process-induced residual stress of variable-stiffness composite laminates during cure, Composite Structures 204 (2018) 12–21.

[54] W. Zhao, K. Singh, R. K. Kapania, Thermal buckling analysis and optimization of curvilinearly stiffened plates with variable angle tow laminates, Journal of Spacecraft and Rockets 56 (2019) 1189–1204.

[55] X. Y. Zhou, X. Ruan, P. D. Gosling, Thermal buckling optimization of variable angle tow fibre composite plates with gap/overlap free design, Composite Structures 223 (2019).

[56] B. Devarajan, R. K. Kapania, Thermal buckling of curvilinearly stiffened laminated composite plates with cutouts using isogeometric analysis, Composite Structures 238 (2020).

[57] M. W. Hyer, Stress analysis of fiber-reinforced composite materials, McGraw-Hill, Boston, 1st edition, 1998.

[58] J. N. Reddy, Mechanics of laminated composite plates and shells theory and analysis, CRC Press, New York, 2nd edition, 2004.

[59] T. H. Dawson, Theory and practice of solid mechanics, Plenum Press, New York, 1st edition, 1976.

[60] E. Lamacchia, A. Pirrera, I. V. Chenchiah, P. M. Weaver, Morphing shell structures: A generalised modelling approach, Composite Structures 131 (2015) 1017–1027.

[61] A. Haldar, R. M. J. Groh, E. Jansen, P. M. Weaver, R. Rolfes, An efficient semi-analytical framework to tailor snap-through loads in bistable variable stiffness laminates, International Journal of Solids and Structures 195 (2020) 91–107.

[62] N. I. Mushelishvili, Some basic problems of the mathematical theory of elasticity, Noordhoff, Groningen, 2ed edition, 1953.

[63] Y. C. Fung, Foundations of Solid Mechanics, Prentice-Hall, New Jersey, 1st edition, 1965.

[64] Y. Tang, X. Wang, Buckling of symmetrically laminated rectangular plates under parabolic edge compressions, International Journal of Mechanical Sciences 53 (2011) 91–97.

[65] K. Washizu, Variational methods in elasticity and plasticity, Pergamon Press, Oxford, 2nd edition, 1975.

[66] J. Woo, S. A. Meguid, J. C. Stranart, K. M. Liew, Thermomechanical postbuckling analysis of moderately thick functionally graded plates and shallow shells, International Journal of Mechanical Sciences 47 (2005) 1147–1171.

[67] H.-T. Thai, S.-E. Kim, Closed-form solution for buckling analysis of thick functionally graded plates on elastic foundation, International Journal of Mechanical Sciences 75 (2013) 34–44.

[68] J. Torabi, R. Ansari, R. Hassani, Numerical study on the thermal buckling analysis of cnt-reinforced composite plates with different shapes based on the higher-order shear deformation theory, European Journal of Mechanics - A/Solids 73 (2019) 144–160.

[69] M. R. Prabhu, R. Dhanaraj, Thermal buckling of laminated composite plates, Computers & Structures 53 (1994) 1193–1204.

[70] M. K. Singha, L. S. Ramachandra, J. N. Bandyopadhyay, Thermal postbuckling analysis of laminated composite plates, Composite Structures 54 (2001) 453–458.

[71] Y. Nath, K. K. Shukla, Post-bucking of angle-ply laminated plates under thermal loading, Communications in Nonlinear Science and Numerical Simulation 6 (2001) 1–16.

[72] N. N. Huang, T. R. Tauchert, Thermal buckling of clamped symmetric laminated plates, Thin-Walled Structures 13 (1992) 259–273.

[73] W. Zhao, K. Singh, R. Kapania, Thermo-mechanical buckling of curvilinearly stiffened variable angle tow laminated panels, in: 22nd AIAA International Space Planes and Hypersonics Systems and Technologies Conference, AIAA 2018-5165, Orlando, FL.

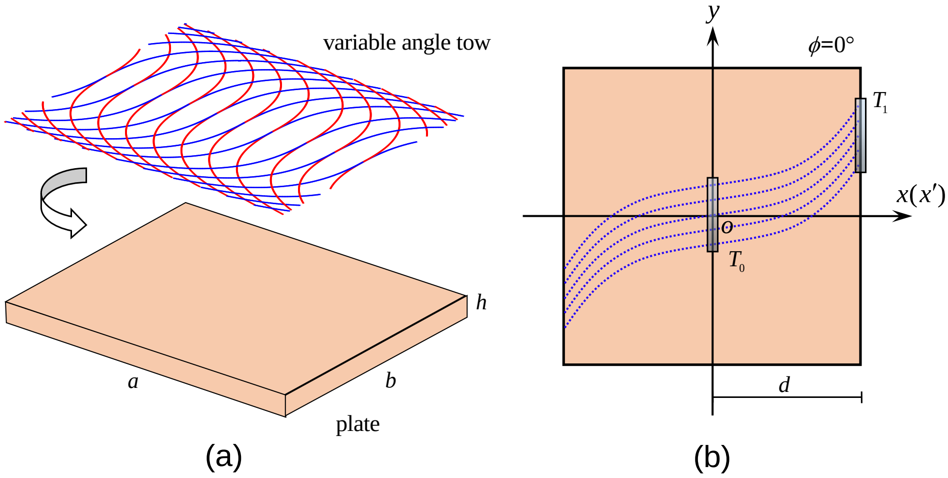

Figure 1: The geometry and layup configuration of a VAT plate: (a) geometric dimension; (b) linear variation of fibre orientation for the case of $\phi = 0°$

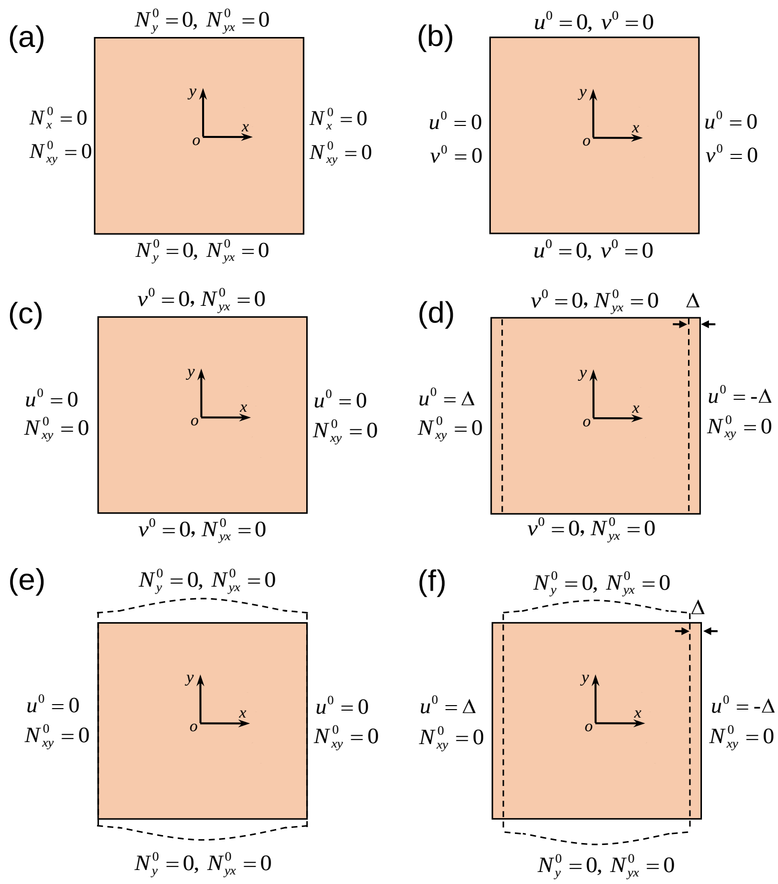

Figure 2: The in-plane boundary conditions and loading cases of VAT composite plates: (a) Type-A: all four edges free of external forces; (b) Type-B: all four edges fixed against both in-plane normal and tangential displacements; (c) Type-C: all four edges restrained against in-plane normal displacements but free to move tangentially; (d) Type-D: uniform end shortening in the longitudinal direction with two transverse edges restrained against normal expansion; (e) Type-E: two longitudinal edges restrained against normal expansion with two transverse edges free to deform; (f) Type-F: uniform end shortening in the longitudinal direction with two transverse edges free to deform

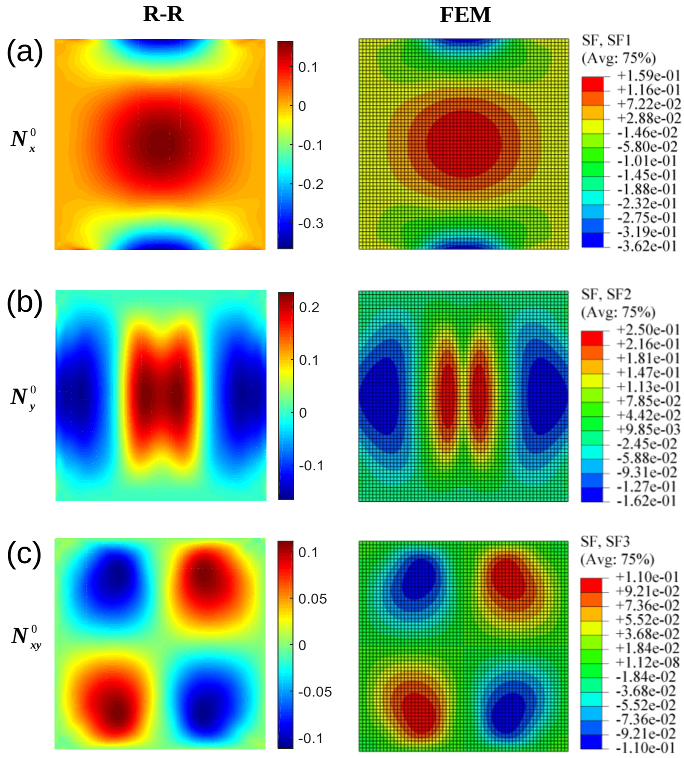

Figure 3: Comparison of FEM and Rayleigh–Ritz results on in-plane force resultant distribution of the VAT plate with linear fibre orientation distribution $[\pm\langle 66.05|11.73\rangle]_s$ under a combination of unit uniform temperature change ($\Delta T = 1°$C) and Type-A boundary constraint (all four edges free of external forces): (a) longitudinal force resultant N_x^0; (b) transverse force resultant N_y^0; (c) in-plane shear force resultant N_{xy}^0

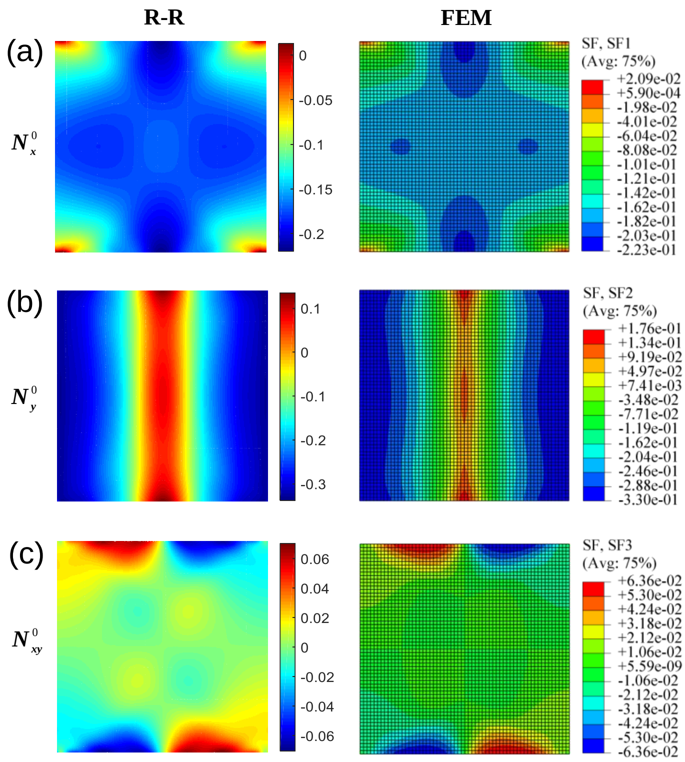

Figure 4: Comparison of FEM and Rayleigh–Ritz results on in-plane force resultant distribution of the VAT plate with linear fibre orientation distribution $[\pm\langle 66.05|11.73\rangle]_s$ under a combination of unit uniform temperature change ($\Delta T = 1°\mathrm{C}$) and Type-B boundary constraint (all four edges fixed against both in-plane normal and tangential displacements): (a) longitudinal force resultant N_x^0; (b) transverse force resultant N_y^0; (c) in-plane shear force resultant N_{xy}^0

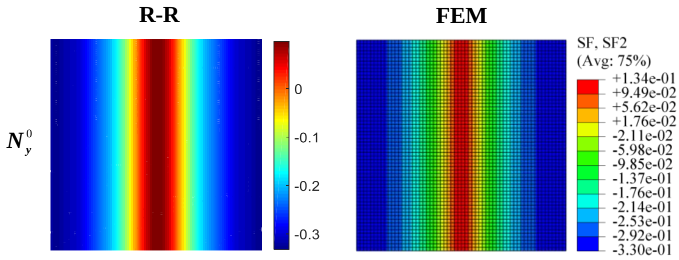

Figure 5: Comparison of FEM and Rayleigh–Ritz results on in-plane transverse force resultant distribution of the VAT plate with linear fibre orientation distribution $[\pm\langle 66.05|11.73\rangle]_s$ under a combination of unit uniform temperature change ($\Delta T = 1°\mathrm{C}$) and Type-C boundary constraint (all four edges restrained against in-plane normal displacements but free to move tangentially)

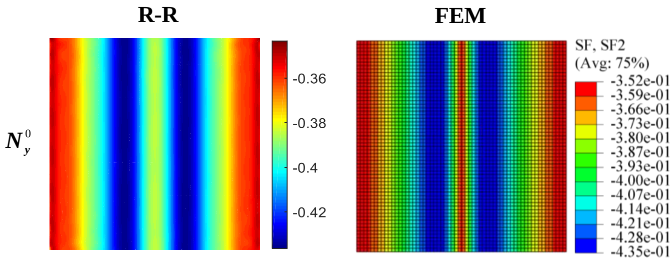

Figure 6: Comparison of FEM and Rayleigh–Ritz results on in-plane transverse force resultant distribution of the VAT plate with linear fibre orientation distribution $[\pm\langle 66.05|11.73\rangle]_s$ under a combination of unit uniform temperature change ($\Delta T = 1°\text{C}$) and Type-D boundary constraint (uniform end shortening $\Delta = 1.0 \times 10^{-3}$mm in the longitudinal direction with two transverse edges restrained against normal expansion)

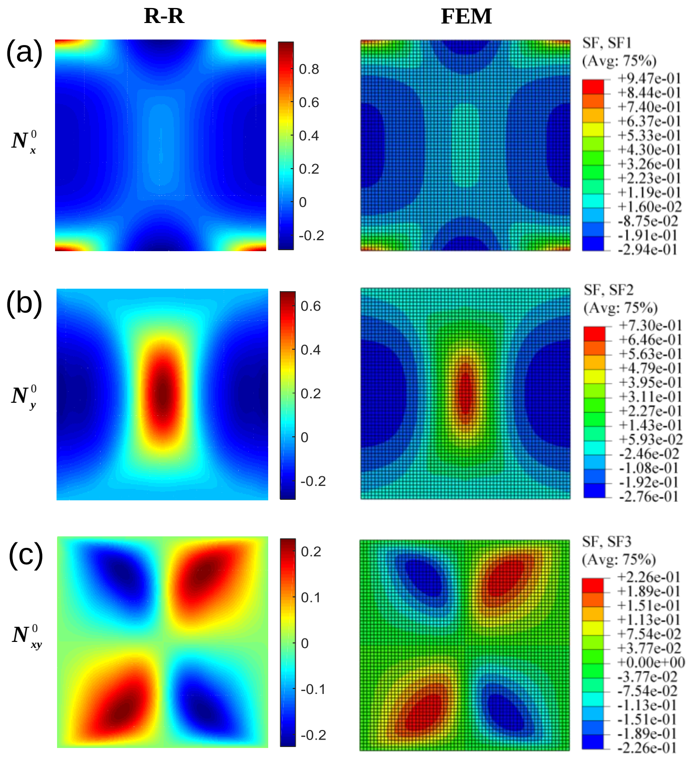

Figure 7: Comparison of FEM and Rayleigh–Ritz results on in-plane force resultant distribution of the VAT plate with linear fibre orientation distribution $[\pm\langle 66.05|11.73\rangle]_s$ under a combination of unit uniform temperature change ($\Delta T = 1°\text{C}$) and Type-E boundary constraint (two longitudinal edges restrained against normal expansion with two transverse edges free to deform): (a) longitudinal force resultant N_x^0; (b) transverse force resultant N_y^0; (c) in-plane shear force resultant N_{xy}^0

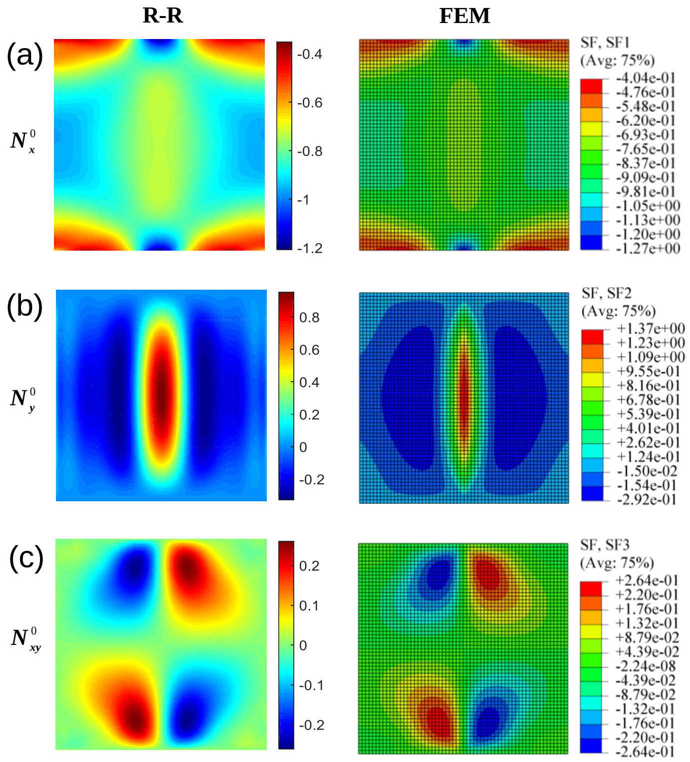

Figure 8: Comparison of FEM and Rayleigh–Ritz results on in-plane force resultant distribution of the VAT plate with linear fibre orientation distribution $[\pm\langle 66.05|11.73\rangle]_s$ under a combination of unit uniform temperature change ($\Delta T = 1°\mathrm{C}$) and Type-F boundary constraint (uniform end shortening $\Delta = 5.0 \times 10^{-3}$mm in the longitudinal direction with two transverse edges free to deform): (a) longitudinal force resultant N_x^0; (b) transverse force resultant N_y^0; (c) in-plane shear force resultant N_{xy}^0

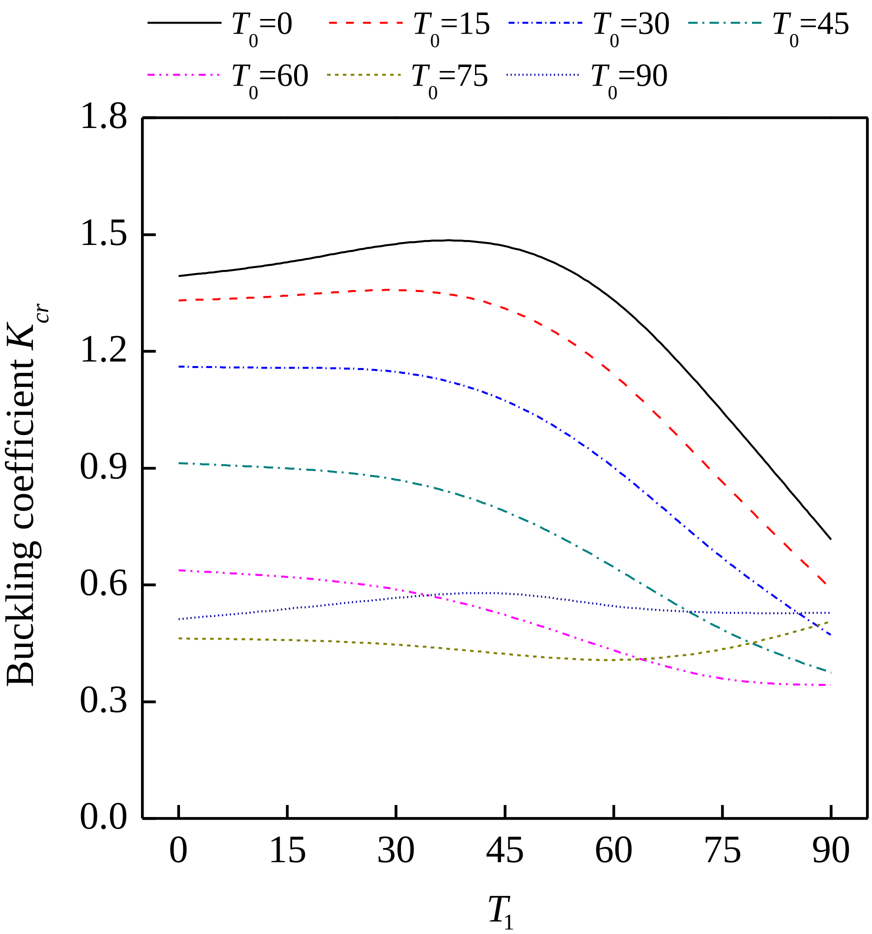

Figure 9: Buckling coefficients of simply supported VAT composite plates with various layup configurations $[\phi \pm \langle T_0|T_1\rangle]_s$ for a combination of plate-type $\phi = 0°$ and temperature $\Delta T = -200°$C. (Each curve in the figure represents a series of VAT panels generated by varying T_1 from 0° at the left-end to 90° at the right-end, but with a same value of T_0, which is labelled in figure)

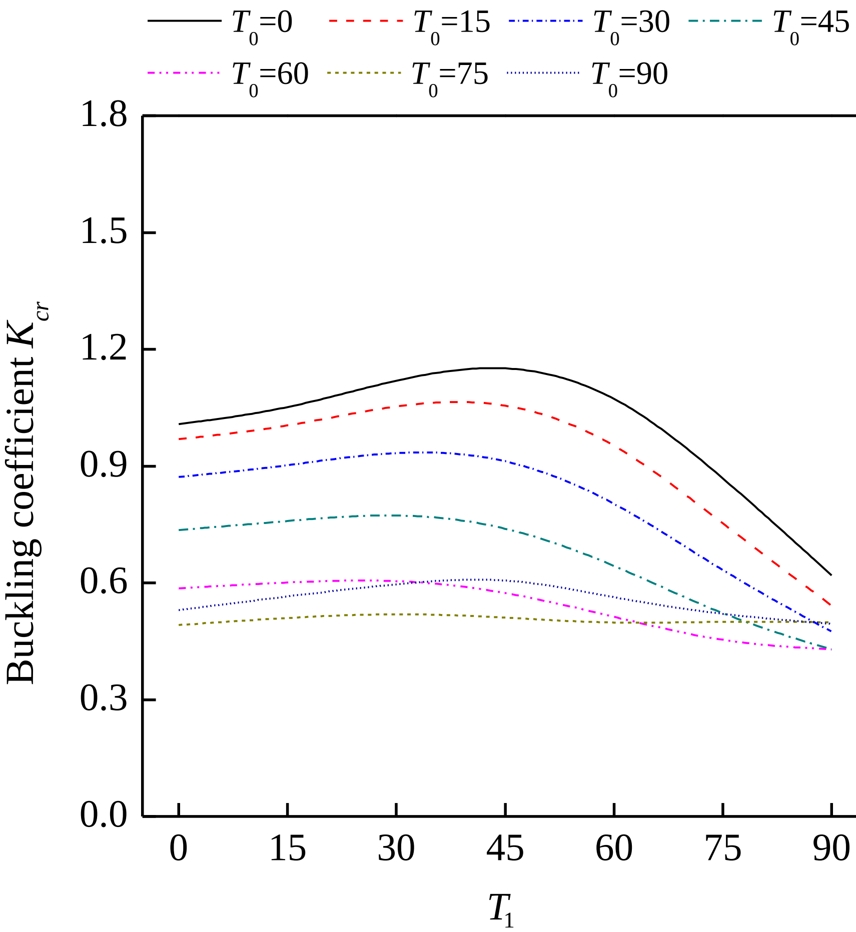

Figure 10: Buckling coefficients of simply supported VAT composite plates with various layup configurations $[\phi \pm \langle T_0|T_1\rangle]_s$ for a combination of plate-type $\phi = 0°$ and temperature $\Delta T = 0°$C. (Each curve in the figure represents a series of VAT panels generated by varying T_1 from $0°$ at the left-end to $90°$ at the right-end, but with a same value of T_0, which is labelled in figure)

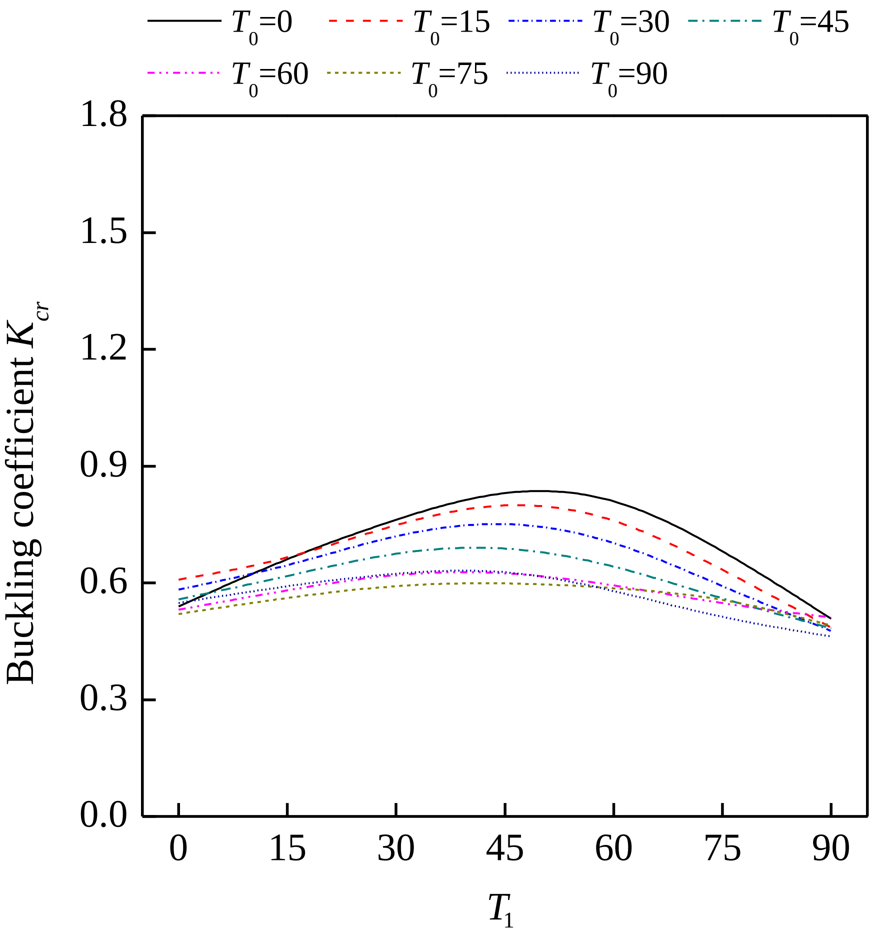

Figure 11: Buckling coefficients of simply supported VAT composite plates with various layup configurations $[\phi \pm \langle T_0|T_1\rangle]_s$ for a combination of plate-type $\phi = 0°$ and temperature $\Delta T = 200°\text{C}$. (Each curve in the figure represents a series of VAT panels generated by varying T_1 from 0° at the left-end to 90° at the right-end, but with a same value of T_0, which is labelled in figure)

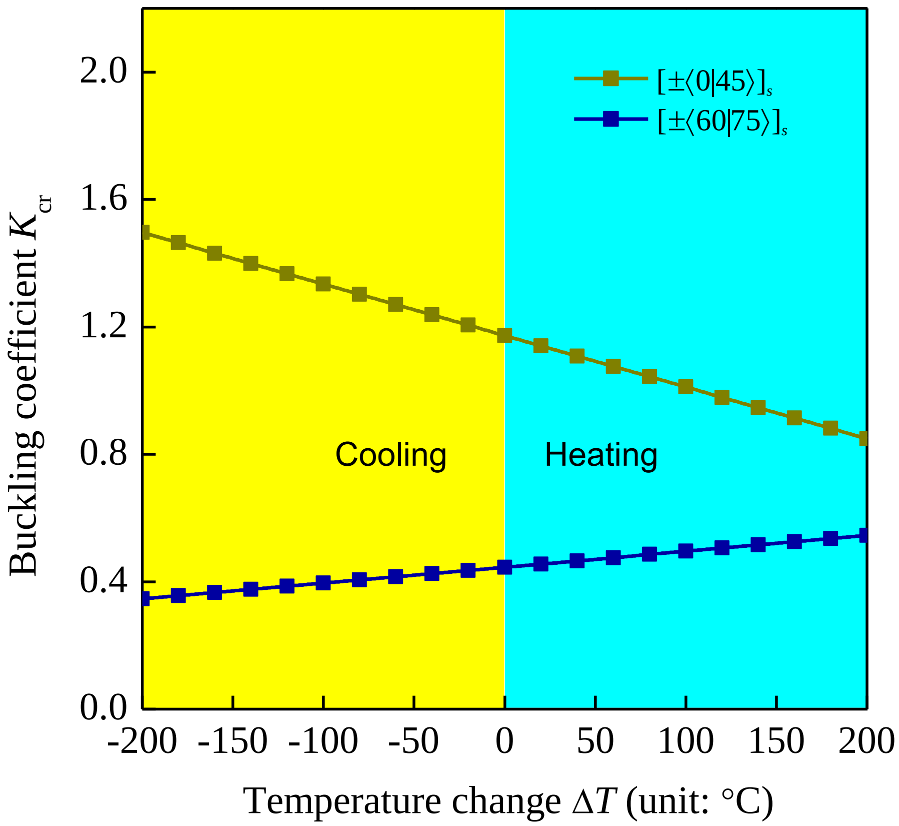

Figure 12: The variation of buckling coefficient K_{cr} with temperature change ΔT for simply supported VAT composite plates with two different layup configurations, that is, $[\pm\langle 0|45\rangle]_s$ and $[\pm\langle 60|75\rangle]_s$. (The blue and yellow areas represent the heating and cooling temperatures with respect to the reference temperature, respectively)

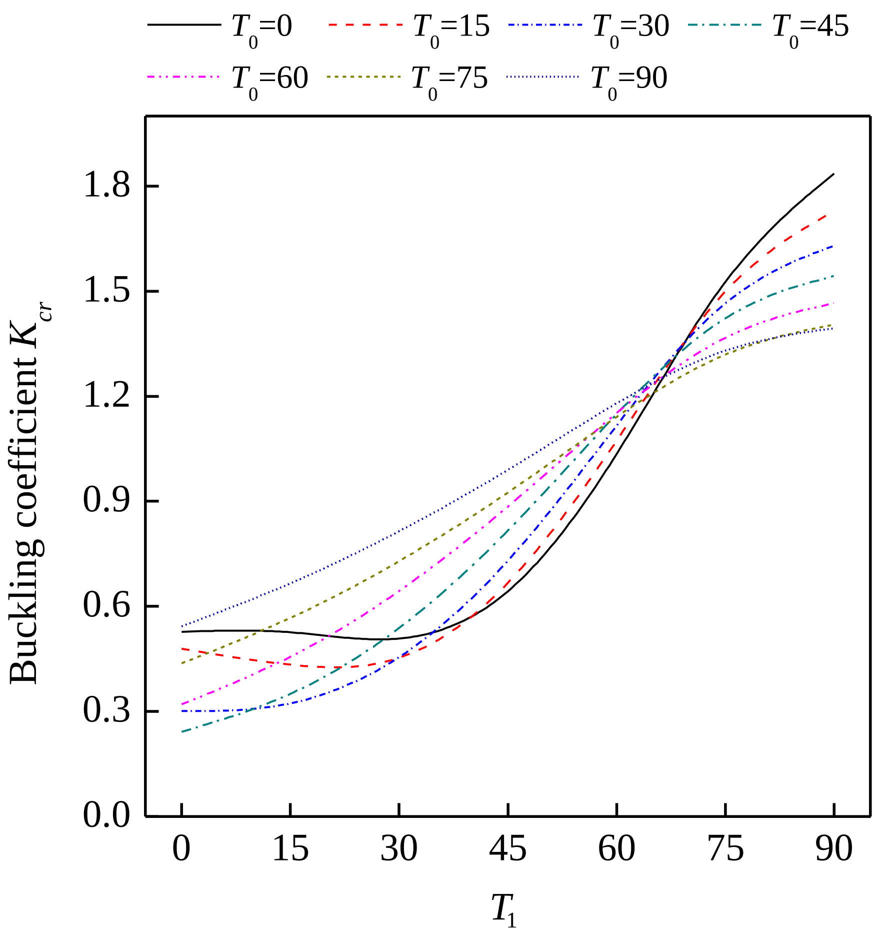

Figure 13: Buckling coefficients of simply supported VAT composite plates with various layup configurations $[\phi \pm \langle T_0|T_1 \rangle]_s$ for a combination of plate-type $\phi = 90^\circ$ and temperature $\Delta T = -200^\circ$C. (Each curve in the figure represents a series of VAT panels generated by varying T_1 from 0° at the left-end to 90° at the right-end, but with a same value of T_0, which is labelled in figure)

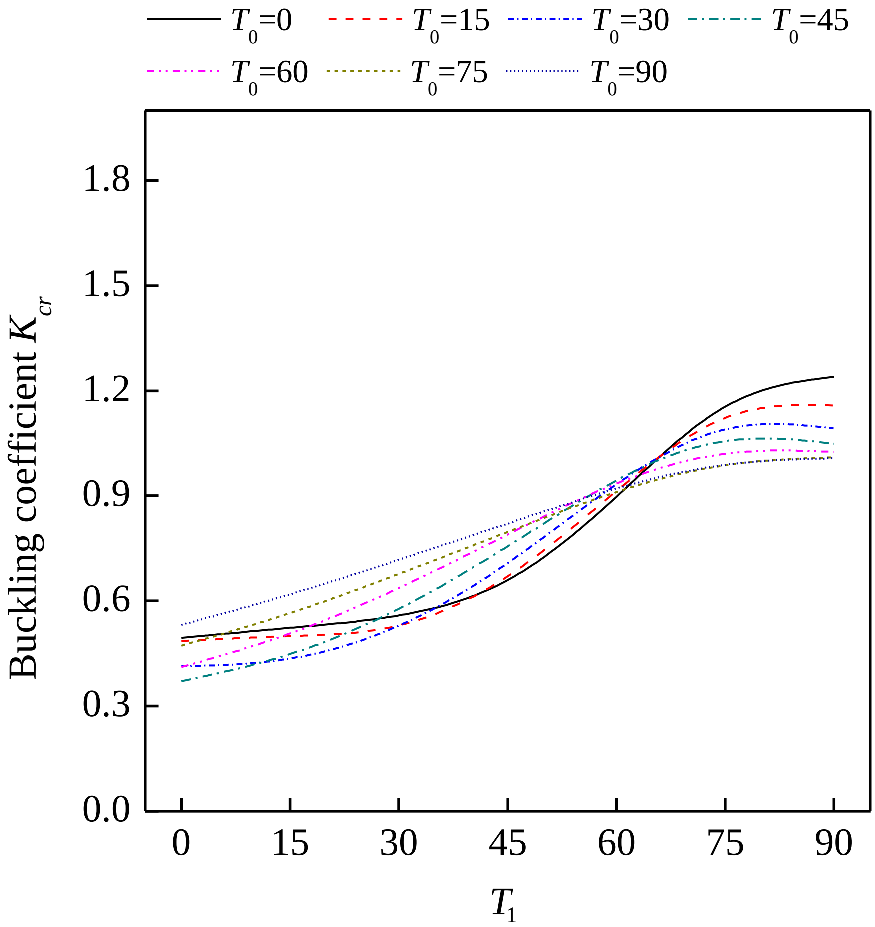

Figure 14: Buckling coefficients of simply supported VAT composite plates with various layup configurations $[\phi \pm \langle T_0|T_1\rangle]_s$ for a combination of plate-type $\phi = 90°$ and temperature $\Delta T = 0°$C. (Each curve in the figure represents a series of VAT panels generated by varying T_1 from 0° at the left-end to 90° at the right-end, but with a same value of T_0, which is labelled in figure)

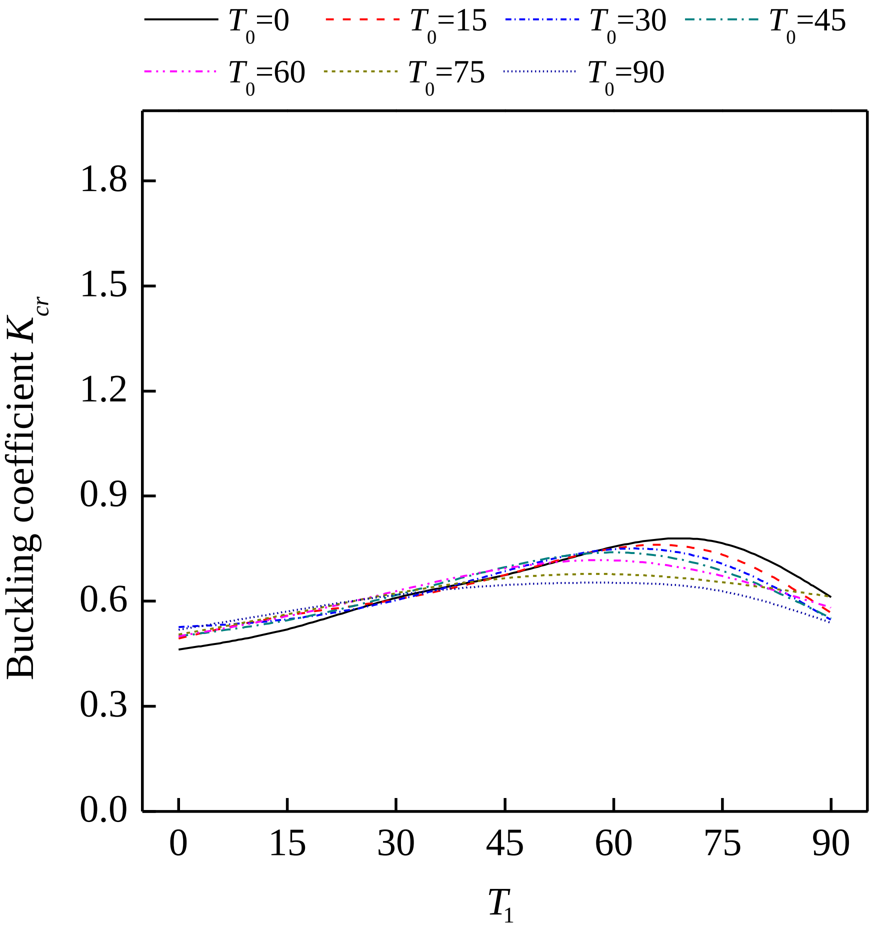

Figure 15: Buckling coefficients of simply supported VAT composite plates with various layup configurations $[\phi \pm \langle T_0|T_1\rangle]_s$ for a combination of plate-type $\phi = 90°$ and temperature $\Delta T = 200°$C. (Each curve in the figure represents a series of VAT panels generated by varying T_1 from 0° at the left-end to 90° at the right-end, but with a same value of T_0, which is labelled in figure)

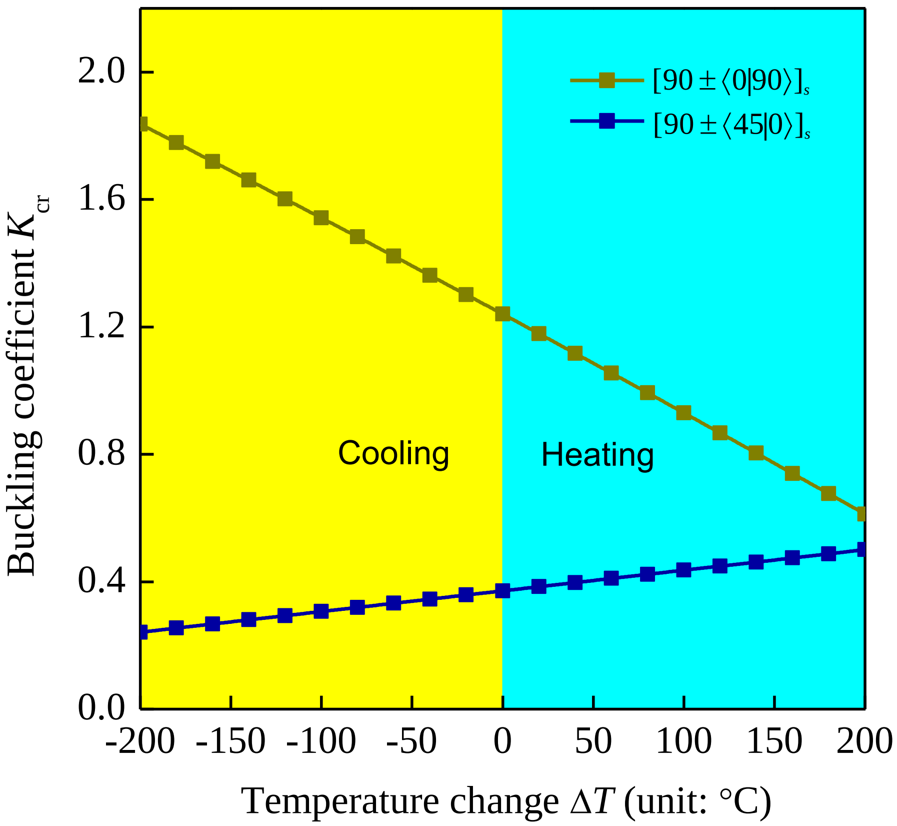

Figure 16: The variation of buckling coefficient K_{cr} with temperature change ΔT for simply supported VAT composite plates with two different layup configurations, that is, $[90 \pm \langle 0|90 \rangle]_s$ and $[90 \pm \langle 45|0 \rangle]_s$. (The blue and yellow areas represent the heating and cooling temperatures with respect to the reference temperature, respectively)